BENDING AND FORCE RECOVERY IN POLYMER FILMS AND MICROGEL FORMATION

A Thesis
Submitted to the Graduate Faculty
of the
North Dakota State University
of Agriculture and Applied Science

By

Theresa Marie Elder

In Partial Fulfillment of the Requirements
for the Degree of
MASTER OF SCIENCE

Major Program:
Materials and Nanotechnology

August 2017

Fargo, North Dakota

North Dakota State University
Graduate School

Title

BENDING AND FORCE RECOVERY IN POLYMER FILMS AND MICROGEL FORMATION

By

Theresa Marie Elder

The Supervisory Committee certifies that this ***disquisition*** complies with North Dakota State University's regulations and meets the accepted standards for the degree of

MASTER OF SCIENCE

SUPERVISORY COMMITTEE:

Andrew B. Croll
Chair

Erik Hobbie

Yechun Wang

Approved:

November 14, 2017 — Date

Erik Hobbie — Department Chair

ABSTRACT

To determine correlation between geometry and material three different model films: polymethylsiloxane (PDMS), polystyrene (PS), and polycarbonate (PC), were singly bent and doubly bent (forming D-cones). Bends were chosen as they are fundamental in larger complex geometries such as origami and crumples. Bending was carried out between two plates taking force and displacement measurements. Processing of data using moment equations yielded values for bending moduli for studied films that were close to accepted values. Force recovery showed logarithmic trends for PDMS and stretched exponential trends for PS and PC. In a separate experiment a triblock copolymer of polystyrene–polyacrylic acid–polystyrene was subjected to different good and bad solvent mixing with any resulting particle morphology examined. Particles formed more uniformly with high water concentration, particles formed with high toluene concentration and agitation yielded three separate morphologies.

ACKNOWLEDGEMENTS

This research was made possible by the NDSU Materials and Nanotechnology Graduate School and the Air Force Office of Scientific Research of the United States. My group including Dr. Andrew Croll, Timothy Twohig, Dr. Damith Rozairo, Dr. Nasibeh Hosseini, and previous members including Dr. Bekele Gurmessa also made this research possible and provided invaluable consultation. Acknowledgement also goes to summer high school students, especially Alex Rice. Characterization methods: NDSU Electron Microscopy lab for use of SEM microscopy with Scott Payne, R1 research lab for use of pull tester and AFM, and Veterinary Diagnostic lab for DIC imaging.

DEDICATION

I dedicate this work to all those who were close to and tolerated me prior to and for the duration of this project and thesis: my parents, my family, my friends, my colleagues, and my adorable cats. I dedicate this work to those who have supported me in one way or another over the course of this journey. Among my family that I dedicate this to are my parents, Bessie and Tony, and their spouses Corey Elletson and Chantal Elder respectively, my brother Craig Elder and his wife Megan, my sisters by marriage and in spirit Cassandra Lucero and Ginette Castaneda and their families, my uncle Tim Carr, and my grandparents, Richard and Beverly Elder, Rosalyn and Deke, Grandma Renee, Harry and Lucy Moss, and Karen Elletson. I also dedicate this work to my wonderful pets, my cats Morgan and Prince, as well as those past, yet to come, and those of friends, family members, and strangers that I have bonded with. I also dedicate this to all of my wonderful friends many of which are like family to me, including Lydia Kelley, her mother Lodema, and the Kelley family, Karen Ufert and her family, Soodabeh Einharjar, Sharonda Fudge, Marie Davis, Nicole Jean, Erica Gee, Jo Nikole, Linda Berry, Kenya Kraft, Cassy, Jah Son, Sita Prakash, Terrance, Kami, and numerous others whom time and space does not allow me to explicitly name, but that I treasure and include in this list. I would also like to thank all of my professors and teachers, both undergraduate and graduate, for their tutelage, especially: Dr. Andrew Croll, my research mentor, who accepted me into his group and guided me along the way, my committee members Dr. Erik Hobbie and Dr. Yechun Wang, and Dr. Ryan Winburn, my undergraduate research mentor. My colleagues and fellow graduate students also deserve to be listed in this dedication for their consultations and social presence: Timothy Twohig, Dr. Nasibeh Hosseini, Dr. Damith Rozairo, Jamie Froberg, Sam Brown, and everyone else that I encountered during the time of my studies that assisted me in some way.

TABLE OF CONTENTS

LIST OF FIGURES

LIST OF ABBREVIATIONS

DNA.....Deoxyribonucleic acid.

1D.....One dimensional.

2D.....Two dimensional.

3D.....Three dimensional.

PS.....Polystyrene.

PC.....Polycarbonate.

PDMS.....Polydimethylsiloxane.

MPa.....Mega Pascal.

GPA.....Giga Pascal.

g.....gram(s).

s.....second(s).

mm.....millimeter(s).

cm.....centimeter(s).

μm.....micrometer(s).

ASTM.....American Society for Testing and Materials.

D-cone.....Developable cone.

min.....minute(s).

°C.....Degrees Celsius.

pH.....Potential of Hydrogen.

DVB.....Divinylbenzene.

PNIPAM.....Poly(N-isopropylacrylamide).

PAA.....Polyacrylic acid.

PS-b-PAA.....Polystyrene-block-poly(acrylic acid).

Mn.....Number average molecular weight.

PDI .....Polydispersity index.

THF .....Tetrahydrofuran.

DMF .....N,N-Dimethylformamide.

MΩ .....megohm(s).

mL .....milliliter(s).

AFM .....Atomic Force Microscope.

MS .....Master Solution.

SEM .....Scanning Electron Microscope.

Si .....Silicon.

DIC .....Differential Interference Contrast.

LIST OF SYMBOLS

T_g .....Glass transition temperature,

T_m .....Melting temperature.

$\varepsilon(t)$.....Strain as a function of time.

σ_0.....Initial stress.

$J(t)$ .....Material compliance as a function of time.

$\sigma(t)$ .....Stress as a function of time.

ε_0 .....Initial strain.

$G(t)$.....Material stiffness as a function of time.

σ .....Stress.

F .....Force.

A.....Area.

ε_{ik} .....Strain along the i and k axes.

x_k .....Coordinate axis of displacements in k.

x_i .....Coordinate axis of displacements in i.

u_k .....Displacement along k axis.

u_i .....Displacement along i axis.

ε.....Strain.

E .....Young's modulus.

ν .....Poisson's ratio.

σ_{xx} .....Stress in x direction.

ε_{xx} .....Strain in x direction.

ε_{yy} .....Strain in y direction.

ε_{zz}.....Strain in z direction.

M_{tot} .....Total moment.

ε_t .....Strain in transverse direction.

ε_l.....Strain in longitudinal direction.

R.....Radius of curvature.

I_x .....Cross sectional area.

t.....Thickness.

b .....Width.

B.....A parameter in moment equation that includes the thickness.

U_s .....Stretching energy.

E_s.....Stretching stiffness.

γ .....In plane strain.

ΔS.....Area of stretched region.

U_b .....Bending energy.

E_b .....Bending modulus.

κ .....Mean curvature in D-cone core.

R_c .....Radius of D-cone.

Φ .....Angle of D-cone formed.

R_s .....A measurement of the sheet.

Φ_2.....Flory particle swelling.

X.....Cross-links within a volume of collapsed particle.

V_c .....Volume in a collapsed particle.

X_{12}.....Flory solvent-polymer interaction parameter.

INTRODUCTION

Polymers

Polymers are a type of soft condensed matter with growing importance in our daily lives[1]. Polymers, natural and synthetic, are in use in technology, buildings, paints, vehicles, medical devices[2], clothing, and food. Natural polymers include silk, cotton, cellulose[3], DNA, proteins, and polysaccharides[1]. Synthetic polymers include polystyrene, polyethylene, Kevlar, polycarbonate, nylon, and siloxanes. Solids made from polymers can have a multitude of dimensions as they can be molded into shapes, fibers, and thick coatings using a variety of methods including: injection molding, thermoforming, blow molding, sintering, and extrusion[3]. Understanding these polymers and how they react to strain and other processes is useful as they continue to infiltrate all aspects of daily life.

A polymer is a macromolecule composed of repeating units of smaller molecules called monomers. Monomers are covalently or physically bonded together forming a chain which can be variable in length, composition, and architecture. Monomers that can be polymerized generally fall into one of three categories: those containing double or triple bonds, those having functional end groups, or cyclic molecules. Double and triple bonds can break to form two new bonds to other molecules and perpetuate polymer growth. Cyclic molecules are similar in that a bond can break between two elements in a ring, incorporating a growing polymer or other monomers. Monomers that have functional end groups can react with the functional end groups of other monomers to bond together and perpetuate the chains. A polymer comprised of only one type of monomer is a homopolymer. A polymer comprised of more than one monomer is known as a copolymer. Polymers come in a number of different architectures based on monomer and initiator reactivity including: chain, branched, grafted, star, and crosslinked[3,4].

Copolymers are differentiated by their monomer arrangements in relation to each other. If the unlike monomers alternate uniformly one after another the polymer is known as an alternating copolymer. Random copolymers are those where the arrangement of monomers are randomly dispersed throughout the polymer with no specific pattern. If two lengths of different homopolymer are bound together the resulting polymer is referred to as a block copolymer. An amphiphilic copolymer can be created when a block of homopolymer that is hydrophobic connects to a block of homopolymer that is hydrophilic[4]. Amphiphilic polymers have a tendency to minimize contact in poor solvents, aggregating with other polymer and molecules in order to minimize surface area that can interact with the poor solvent[1,2,3].

The versatility of polymeric materials arises from their unique physical and chemical properties attributable to their large length scales and high molecular weights. The large number of atoms in a polymer exponentially increases weak intermolecular forces: van der Waals, H-bonding, ionic forces, and dispersion forces; rather than chemical forces and potentials that dominate individual and small molecule interactions[4]. These forces can lead to polymer entanglement with themselves and other polymers, complex arrangements similar to tangled cords which restrict individual polymer movements. The restriction of motion is often depicted as a tube at any given time; the polymer is confined to moving only within the tube as the surrounding polymer and weak forces limit the space it can occupy at that given time. With enough time the polymer might reptate out of its particular tube or the tube might change dimensions as the entire system is in motion, rearranging while in solution or above the polymer's glass transition temperature (T_g)[1].

Polymer melts are considered "fragile liquids" with significant increases in viscosity as the temperature of the system decreases[5]. Melts are polymer systems above a certain

temperature, the melt temperature, T_m[6]. The behavior of homopolymer melts resembles that of ideal gases as intermolecular and intramolecular forces dominate over fluctuations in density[8] at any given point in the system. This assumed ideal of identical interactions between ideal chains approximate experimental behaviors in bulk accurately[9]. Melts with less volume might deviate from ideal behavior[8]. In fluid polymer systems, melts and solutions, there is freedom of movement for monomers around their bonds; therefore, the polymers assume different conformational states such as helices and coils[7].

Polymer solutions are polymer systems in solvents that do not exhibit melt behavior, the solvent affects monomer interactions either through increasing or decreasing contact with neighboring monomers. Polymers in solution exhibit excluded volume effects where a neighbor monomer cannot occupy a certain area of space due to it being occupied by another monomer or solvent molecules[7]. Monomers might have frictional interactions with neighboring monomers when in good solvents[10]. In good solvents the monomers are also surrounded by shells of solvent molecules that expand the chain away from other monomers and increase the overall area occupied by the polymer chains. These are called expanded chains[7]. Polymers in bad solvents will experience aggregation as solvent molecules and monomer prefer contact with themselves and try to reduce surface contact with each other[1,7].

Polymer chains can link together in numerous places to form macroscopic molecules. The bonding of neighbor chains through covalent bonds, reversible physical bonding such as entanglements or through linker molecules is known as crosslinking[1]. Crosslinking greatly changes the properties of the material by increasing molecular weight, increasing thermal stability, and changing stress-strain dynamics. As neighboring polymers crosslink together forming a network the macromolecule grows, increasing in molecular weight and reducing

solubility. Thermal stability is increased due to a higher number of bonds that would need to break in order to separate molecules leading to a built in redundancy that improves mechanical properties. For physically crosslinked polymers the material might have the beneficial possibility of self-healing through the reforming of bonds under the right conditions[11].

The density of crosslinking distinguishes if the resulting macromolecule is a gel, elastomer, or resin. Gels are loosely crosslinked and can absorb solvents readily resulting in swelling. Elastomers vary in crosslink density and show varied response to stress and stretching based on the degree of crosslinking. Gum is a natural elastomer of cellulose micro fibrils[1] which have fewer cross-link bonds than a commercial rubber elastomer which imparts greater stretching and self-healing properties but higher malleability under stress loads. Many commercial elastomers are more highly crosslinked resulting in a more fixed shape and lower mobility under stress with higher recovery of the original dimensions after the stress stimulus is removed[2]. The often desirable reversible reaction to stress (elastic stretching) can be as large as 500% and 1000% of initial length due to a low modulus that increases as strain increases. Elastomer strength can be increased through the addition of reinforcing inorganic fillers, large quantities of nano-sized particles that do not participate in cross-linking[12], make a filled elastomer. The most highly crosslinked macromolecules are resins which are similar to typical hard solids in their hardness, resiliency to heat[3], and high tensile strength[13]. Unlike other less crosslinked polymer networks, resins do not easily absorb solvent[3] and are resilient to chemicals[14].

Some polymers have been shown to crystallize at low temperatures, below T_m, exhibiting both crystalline hierarchical ordered structures and interspersed amorphous regions. The amorphous regions result from irregularities and defects of packing as polymers crystallize

through folding sections of their chains into folded-chain lamella structures. The folding must occur around entanglements with themselves and neighbor polymers; kinetics more than thermodynamic equilibriums determine the resulting crystalline morphology[1]. Methods of crystallization that maintain temperatures close to melting point or melt temperatures for extended periods of time result in more highly ordered crystallization than those where quenching halts polymer folding prematurely. The degree of crystallinity imparted also depends on the polymer composition as monomers that are less bulky or have larger attractive forces guiding them into crystallization will crystallize more readily than those lacking either condition[3].

Glasses are amorphous like liquids, lacking long range order at high temperatures even if they appear to have order at small scales. Bulky groups keep glassy polymers from uniformity by acting as nucleating clusters[15] that expand, these clusters fit into irregular mosaic arrangements[5] rather than ordered arrangement. Glass formation can also be related to voids between monomers being occupied by solvents, or other molecules[5] which alters polymer motion. The transition into a glass from a solution or melt is characterized by a temperature, T_g the temperature at which the system has a low kinetic energy and begins to solidify[1,16]. T_g can be thickness dependent with thinner polymer systems having a lower or higher T_g due to increased heat diffusion and higher surface area to volume ratios than polymer in bulk[17]. Substrate effects can also lower or raise T_g from attractive or repulsive forces that alter mobility[18].

The effect entanglement has on polymer solution and melt mechanical properties are increased viscoelasticity, resistance to shear forces[1], and non-Newtonian viscosity. At low density of entanglement the viscosity is high while at high density the behavior is elastic[19]. In solutions of good solvent certain polymers show rod-like behavior of monomers[15]. Polymer

systems show non-Newtonian variable viscosity under shear due to chain stretching and entanglements which lead to shear-thinning or shear-thickening rheological behavior[20]. Fracture appearing as macroscopic discontinuity, even in highly dense systems experiencing shear or in melts are rare[19]. For most practical purposes, it is more valuable to know the mechanical properties of polymer solids. Generally polymeric solids respond to stress as shown in Figure 1. There is a linear response to stress at low deformations, a yield peak as polymer chains begin to irreversibly slip past one another, and strain stiffening after polymers reach the limits of extension. As strain stiffening rises, backbone bonds begin to break and the material eventually macroscopically fails.

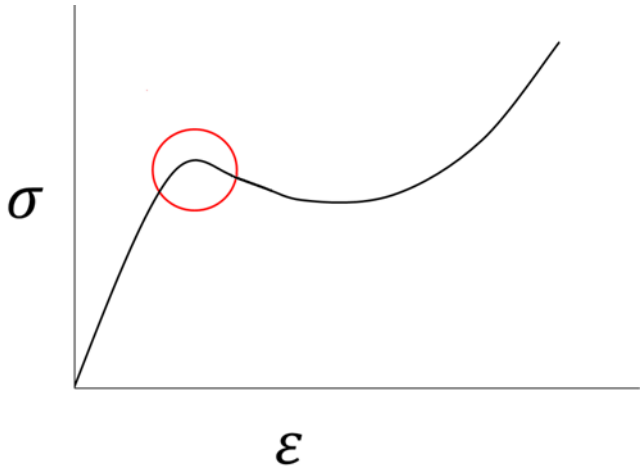

Figure 1. A general schematic curve of stress-strain mechanics in amorphous polymeric solids. Initially there is a Hookean linear slope as polymers begin to straighten. As stress and deformation increase polymers slide past each other and there is a yield peak (circled in red) followed by a drop in stress from the polymers aligning. The stress and strain then rise again as the polymers become fully extended and over extended, an effect known as stiffening.

Failure is damage in a system which can take several forms including buckling, wrinkling, crazing, and fracture. Buckling and wrinkling are out of plane bends formed by a thin material relieving excess strain that result when a critical compressive stress is exceeded. Buckling is on a larger scale than wrinkling which are localized sinusoidal ridge deformations that form from lower strains on lower modulus substrates[21,22]. Crazing is microdefect cracks

whose sides remain connected by polymer fibrils[23]. Fracture is cracks propagating in a material where the two sides are not connected; crazing can progress to fracture when enough stress is applied to break the connecting fibrils[24].

The broad interesting behavior of polymers resulting from their unique properties and the range of polymeric materials that can be made inspired our research. In this thesis polymer film stress response to static and dynamic bending and kinetic microgel assembly will be discussed. We define static bending as bending with incremental equilibrium points from constant speed loading and dynamic bending as constant load non equilibrium bending with changing microscopic arrangement as a result. The thesis is divided into three chapters for clarity. First is a chapter on static and dynamic single bends, in which we bent 2D sheets of polymeric film in our experiment. Specifically the film was deformed at constant speeds between two plates to different maximum displacements. At maximum displacement force recovery over time was measured. Next, is a chapter on static and dynamic double bends introducing the D-cone geometry. Finally, the third chapter is on the formation of microgel particles using amphiphilic block copolymers and a kinetically hindered self-assembly process. Polymeric materials are widely used so further understanding of their engineering properties in bending, under loads, and in microgel particles are useful to their applications and engineering.

CHAPTER 1. STATIC AND DYNAMIC SINGLE BENDS OF POLYMER FILMS

Background

Thin systems with alterable shape are finding new uses in everyday life such as stretchable bio-medical electronics[25,26] including folding biosensors[27,28], gas sensors, artificial muscles, bendable memory devices[29] and phones[30]. The potential for 2D materials that can be turned into 3D materials can be seen in retractable shapeable solar panels and temporary residences[31], foldable or flat-laying structures for use in space[32,33], or in situ medical devices[34]. The ability to stretch, twist, and form shapes can give improved mechanical properties, add functionality, and provide structure dependent attributes[35]: adjustable surface areas[36], additional axes for accuracy in sensors[28], and additional spaces or breaks between regions[29] that can serve many purposes including as fluidic channels[27]. Shapeable systems have the added advantage of cost savings[35] as they can be made from paper[29], graphene[37], fabrics[31], and polymeric materials[27,29,34,35,38]. The multitude of advantages and uses of 2D systems makes understanding their mechanics and force responses useful.

The formation of the thin materials into predetermined geometries can be done in a number of ways; bending and folding such as origami, cutting, or a combination such as kirigami. Bending is a global deformation of a system from linear to a curve induced by moving sections closer together. Folds are localized linear deformations[34] of sharper curvature than bends. Origami is the art of paper folding used to make a shape by stretching and bending a 2D material out of plane[34,37,39,40]. The out of plane bending is often in the form of creases to create defined shapes and increase complexity[34]. Kirigami is similar to origami in that it is a method of folding out of plane, however, it also employs cutting to form complex shapes or to relieve

strain[38]. Crumples which are complex networks of folds, ridges, and creases compressively deform under stress[41,42,43, 44, 45] and can be formed through balling up a material.

A large body of research has formed around the formation of certain shapes, complex and simple, both experimentally and theoretically through origami and kirigami methods. Origami or kirigami designs can be built into a thin material in various ways: selective molding of thin and thick regions[46], built in hinges arranged in tessellated patterns of rigid segments[47,48,49], local modulus variations[25,50], locally induced damage[51], thermal actuation[34], interlocking sections or sections attracted to each other through forces such as magnetism[49], hydrophilic attractions[36], and electrical stimuli[52].

During and after the shape changes the system needs to remain functional[26] as any damage can deplete or prevent functionality[53]. For a number of applications it is also crucial for the shape changes to be able to be formed quickly, reliably[38], with reversibility[34], and stability. The morphology change from one shape to another is a mix of mechanism and structure[35]. The stress-strain response and failure are engineering-relevant properties that are necessary to predict the overall behavior in a system. Our research focuses on the mechanics of structure in conjunction with the material properties of the system[37]. In particular we examine the origami relevant structure, a single bend.

Single bends were chosen as they are non-unique structures that can be used individually or in more complex geometries[49] such as origami and crumples. Bends contain compression and tension[29] around a central neutral axis. Bending mechanics are useful in determination of the maximum stress a system can sustain before failure. Failure can be in the form of fracture[53], buckling, or crazing. As polymeric materials have the potential to satisfy engineering

requirements for shape changing systems at low cost[34,38] we chose to use polymer films in our bending experiments.

A polymer's mechanical utility is determined primarily from its mechanical properties such as its stress-strain responses, which may be complex and contain features such as elastic deformation, flow, and creep[3]. In order to study how these fundamental material properties influence origami structure we chose three different model polymer films. The three different thin polymeric films with varying responses to stress are used to highlight material differences, polystyrene (PS) and polycarbonate (PC), both glassy materials, and polydimethylsiloxane (PDMS), a filled elastomer.

PDMS is used commercially in a variety of products including sealants, biomedical applications, and to create hydrophobic surfaces. It is a hybrid polymer formed from monomers of Dimethysilanediol, an inorganic-organic, that when mixed with a curing agent initiates crosslinking to form a rubber analog[2]. It is considered a flexible filled elastomer and can be stretched[54,55]. Silicones like PDMS are commonly used to surround electronic components due to their insulation qualities[56]. Sylgard 184 PDMS has low hardness with a modulus that increases with increasing curing agent reaching maximum values at a 9:1 polymer to curing agent weight ratio. In our bending experiment we used 10:1 PDMS that has bulk tensile or fracture strength of 2.24 MPa with a Poisson ratio of 0.535, and an elastic modulus of 2.60 MPa[56,57]. The exact material properties are also dependent on curing temperature. The bulk modulus, Young's modulus, ultimate tensile strength, ultimate compressive strength, and compressive modulus vary with curing temperatures between 25-200 °C: 2.20-4.95 GPa , 1.32-2.97 MPa which increases linearly with temperature, 3.51- 7.65 MPa, 51.7-31.4 MPa, 186.9-117.8 MPa, respectively[58].

PS was one of the first polymers synthesized; it is a glassy polymer of styrene monomers with a T_g near 100 °C. PS is in common use in many current applications due to the rigidity and transparency of the polymer when molded. Among the current applications are plastic lenses, toys, disposable dishes and food containers, and electronics. PS due to the packing qualities of the phenyl groups along the C backbone is amorphous and brittle with failure resulting in crazing and cracks[2] when yield strength of 28.7-41.4 MPa[59] is surpassed, lower for films below 100 nm thickness[60]. General purpose polystyrene has a Young's modulus of 3-3.5 GPa , tensile strength of 30-100 MPa[61], flexural strength of 42.06 MPa, flexural modulus of 3.275 GPa, and compressive strength of 99.97 MPa[62].

PC is commonly used in water bottles and food containers as well as bullet-resistant windows. PC like PS is a glassy polymer, composed of two monomers Bisphenol A and Phosgene that link via condensation polymerization. PC is transparent with a high refractive index. PC is less brittle than PS with failure tending toward plastic deformation rather than breakage[2]. PC has Young's modulus of 2.0-2.6 GPa, ultimate tensile strength of 52-75 MPa[58], and fatigue stress of 25-39 MPa[63], maximum stress of 10.40 MPa, yield stress of 61 MPa[64],and yield tensile strength of 58.6-70 MPa[65].

Using these three materials we carried out single bends in order to determine their mechanical properties for wider use in engineering and understanding of the mechanics of simple geometries imposed on a film. The system behavior is a combination of the material properties, structural dimensions, and the stress and strain behavior of the system.

In order to observe any dynamic changes in our model materials we chose to measure force recovery (the displacement is fixed and force is measured as a function of time). The stress-strain behavior of a material can follow several pathways including creep, aging, flow,

elastic recovery, and failure. Under quasi-static loads viscoelastic materials experience the common processes of creep or relaxation which decrease or increase the strain and deformation in a system measured on logarithmic time scales[66]. The pathway that the film takes can predict its long-term behavior in real world applications.

Creep is when a material continues to experience deformation, generally as expansion, while under constant load. This expansion is the result of the material trying to equilibrate strain which comes about from enlarging the area experiencing the load force[67]. As a function of time creep is:

$$\varepsilon(t) = \sigma_0 J(t) \quad (1)$$

where $\varepsilon(t)$ is the strain as a function of time, σ_0 is the initial stress, and $J(t)$ is the material compliance. Creep becomes a constant strain rate after a fast initial elastic response. Flow is similar to creep in more liquid and amorphous materials. Relaxation is the opposite of creep, a strain is applied and held constant and the stress changes as a function of time

$$\sigma(t) = \varepsilon_0 G(t) \quad (2)$$

where $\sigma(t)$ is the stress as a function of time, ε_0 is the initial strain, and $G(t)$ is the stiffness. In relaxation stress often goes to a constant after initial elastic response[68]. A glassy polymeric material that is below its glass transition temperature can have structural relaxation, rooted in molecular rearrangement, which continues indefinitely[69].

Physical aging is the process of slow molecular rearrangements that occurs over time as a system moves from its original state to a lower energy state through repeated 'barrier' transitions. Aging is a gradual process over the course of a material's lifetime that can diminish its functionality[70]. Since aging is a response that can be altered by loads and occurs on large

time scales, we must also measure some form of dynamics, for example relaxation or creep in order to have a full understanding of material and structure.

Theory

The behavior of any material is a combination of its configuration and its basic response to stress and strain. Forming a single bend by confining a thin sheet between two parallel plates forms a particularly simple example that is analogous to simple beam bending and 2D plane deformation.

A stress in a system is defined as the force per unit area acting on some surface:

$$\sigma = \frac{F}{A} \tag{3}$$

where σ is stress, F is a force, and A is the cross sectional area. Strain is:

$$\varepsilon_{ik} = \frac{1}{2}\left(\frac{\partial u_i}{\partial x_k} + \frac{\partial u_k}{\partial x_i}\right) \tag{4}$$

where ε_{ik} is the strain along the i and k axes, x_k and x_i are the coordinate axis of displacements u_i and u_k, respectively. In the 2D case the third plane can be ignored as strain is only along two axes[71,72].

Hookean constitutive equations that relate the stress-strain relationship in Hookean solids under tension or compression (a solid where stress and strain have a proportional linear relationship[73]) are:

$$\sigma_{xx} = \frac{E}{(1+v)(1-2v)}\left[(1-v)\varepsilon_{xx} + v\left(\varepsilon_{yy} + \varepsilon_{zz}\right)\right] \tag{5}$$

and

$$\varepsilon_{xy} = \frac{1+v}{E}\sigma_{xy} \tag{6}$$

where E is Young's modulus, ν is Poisson ratio, and σ_{xx} is the stress in the x direction[72]. Young's modulus is a material property. Poisson's ratio is defined as:

$$\nu = -\frac{\varepsilon_t}{\varepsilon_l} \quad (7)$$

where ε_t is the strain in the transverse direction perpendicular to the direction of force and ε_l is the strain in the longitudinal direction in the direction of force and stretching[74]. Poisson's ratio expresses how much the material's cross-sectional geometry changes proportionally as it is deformed.

A moment is a force acting on a point mass about a center of rotation[73]. The moment is useful in the determination of bending forces as it must sum to zero if the bent object is in equilibrium. The stress and strain are not uniform throughout a bending film. In the bent film there is a neutral central region that is not subjected to bending strain, on either side the film is stretched or compressed accordingly. The integral parameters reflect the distance from the neutral axis based on the neutral axis being half of the thickness of the material. The bending moment, using the plane stress modulus, is defined as:

$$M_{tot} = \int_{-\frac{t}{2}}^{\frac{t}{2}} \int \frac{E}{R} yx dx dx \quad (8)$$

where t is the thickness, R is the radius of curvature, and yx is the cross sectional area which can also be expressed as I_x[72]. The radius of curvature is the radius of the curve or semicircular area formed by the bend. In order to find the change in cross sectional area over the entire material, the entire curve and width of the integral with respect to x (in this instance) is taken to get a total moment. Integration gives:

$$M = \frac{E}{R}\frac{bt^3}{12(1-v^2)} \quad (9)$$

where b is width, the y direction measurement.

Assuming a force has been applied to bend an initially flat sheet to a radius of curvature, R, we can write:

$$M_{tot} \sim FR \quad (10)$$

where M_{tot} is the total moment. A more detailed calculation yields a proportionality constant of $\frac{\pi}{4}$, and the force felt by the plates becomes:

$$\frac{F}{b} = \frac{B\pi}{4R^2} \quad (11)$$

just as in the crushing of a cylinder. Here B is known as the bending modulus and is given by:

$$B = \frac{Et^3}{12(1-v^2)} \quad (12)^{75}.$$

Experiment

Sample Film Preparation

Fabrication of PDMS

Sylgard silicone elastomer base 184 and Sylgard 184 silicone elastomer curing agent (cross linker) were mixed in a 10:1 weight ratio, 2-5g in excess of desired weight needed for all films. The solution was mixed with a glass pipette for 5-10 minutes. Mixed solution was then poured into PS sample containers to a desired weight (3g, 5g, 7g, 10g, 15g, 20g, 25g, and 30g in the current work) or in order to create uniform thickness samples. Much thinner films were produced by flow coating solution onto a mica surface. Sample containers were placed in vacuum at 20-25 in Hg for 5 minutes, repeated for a total of 4 cycles to allow further release of

gas bubbles. Next at 15 in Hg the vacuum oven heat was set to 1 (~ 85 °C) and film allowed to anneal for 90 minutes. Film was removed promptly from the oven and allowed to cool a minimum of 30 minutes prior to use.

Fabrication of PS and PC

Various PS and toluene solutions were created by weight 5%, 20%, and 25% wt. % PS. PC and chloroform solutions were also created to various weight ratios (10% or less). Solutions were left to sit for 48 to 96 hours before use, allowing polymer solutions to fully mix. Freshly cleaved mica was then placed on a glass microscope slide held by the capillary force of a small amount of water.

Dropcasting: Solution was added dropwise to the center of the mica until it spread to the edges without going over the edge. Samples were then places in chambers to slow evaporation and left overnight to dry. In the case of PC the chamber contained excess chloroform and for PS the chamber was in air.

Flowcoating: The solution was placed behind a blade which was then moved at constant velocity from one side of the mica to the other. The blade was kept in close proximity to the mica in order to achieve thin layers of film and allow for the escape of solvent.

Spincoating: Mica and microscope slide were placed on vacuum stage of spin coater. Solution was added dropwise into the center and then spun to spread the solution over the mica.

After sufficient time passed to allow toluene or chloroform to evaporate the film was placed on a hotplate at 150 °C for 90 minutes for PS and 180 °C for 60+ minutes for PC.

Mechanical Testing

Each film was cut into a rectangular shape based on the scale needed. Dimensions were measured with a calipers for length, width, and thickness as in Figure 2 if not too thin; films too

thin to be measured with calipers were measured with confocal microscope. Film was placed between two plates with just enough distance between them to give the film bend a slight curvature, small strips of tape secured ends if needed, mainly for glassy films. The forces and displacement of the film and plates during descent and ascent from desired displacement were observed. The motor was moved at a constant speed to the desired displacement while a video recorded the plate movement and forces as measured at short time scales. After force recovery, if any, the motor was set to return to the start position moving at the same constant speed as during previous step, video was taken of this as well.

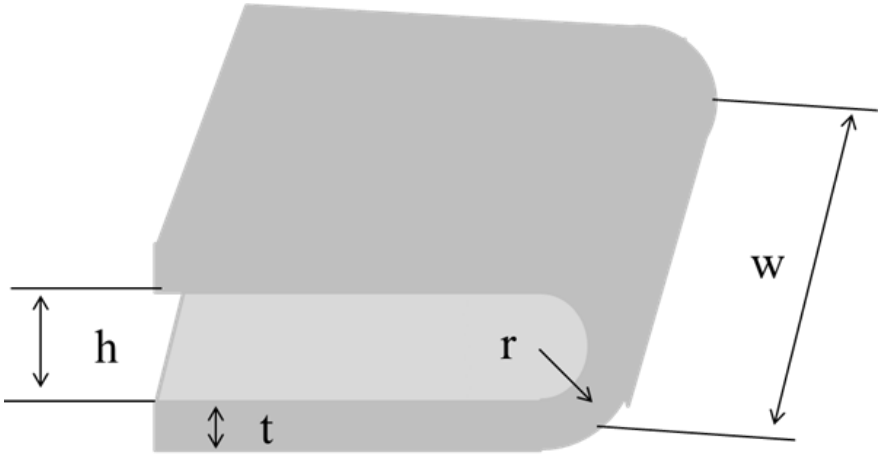

Figure 2. The single bend geometry and dimensional measurements taken of a sample film.

Apparatus

There were two apparatus used in this work. One for the large scale work (in air) and the other on the confocal (films in air or in liquid), however the basic set up was similar for both. The large scale apparatus, Figure 3, used a Denver instruments scale with a glass plate which served as the bottom plate for bending. Two mirrors were set up, one to reflect the mass shown on the scale and the other to reflect the image from the first mirror into the camera. The top plate was a large glass microscope slide epoxied to screws and attached to an actuator and Newport Motion Controller Model ESP 301. ESP software utility program moved top plate up and down

during experimental runs. A ruler was placed beside and aligned to bending film and plates to track plate calibrate distances. A telescope attachment and Pixelink 954000025 camera were used to get clear bright picture prior to video or picture capture using PixeLINK software.

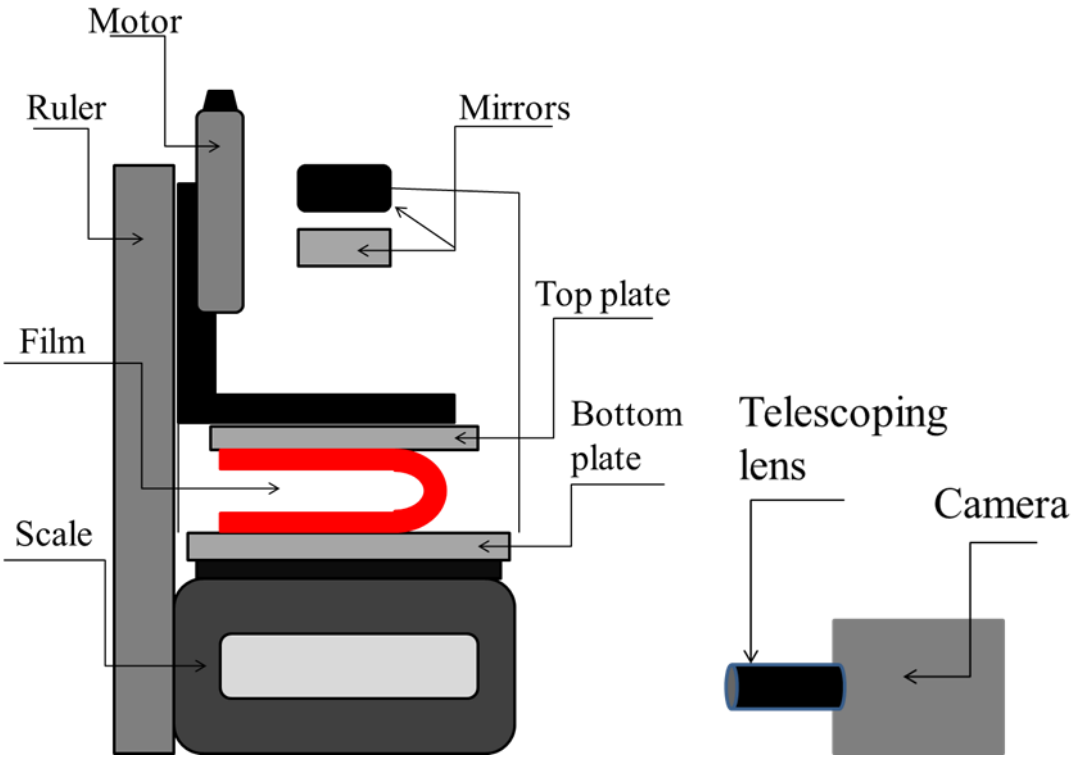

Figure 3: Large scale apparatus for two plate bending used in this work. The bottom plate is stationary atop a scale while the top plate is attached to a motor and mobile. A telescoping lens and mirrors allow for the film and scale numbers to be in focus. The ruler on the side is for calibrated tracking of plate distances.

Analysis Tracker

Photo and video data were obtained from PixeLINK camera software and analyzed with Tracker program by Doug Brown. A calibration stick was set up using the reference ruler and points on both top and bottom plates were tracked to determine the distance between plates at each time point. The mass was then taken from the picture of the scale for individual video frames. The data was placed in an Excel file where it was converted into values obtained of force in Newton and displacement in cm.

Tensile Test on PDMS

PDMS has known mechanical properties; however, there have been found to be variations in bulk properties such as modulus based on crosslinking ratio and temperature of curing, linear dependence[58]. To find the modulus for our samples we ran an ASTM tensile dogbone T-test. A dumbbell or dogbone shape, Figure 4, with two wide regions and a narrow central region was cut out from PDMS films with a cookie cutter. Measurements of length, width, and thickness were taken before stretching, at the max point, and after return to start position. Wide parts of film were clamped in and program was set to a speed and distance. Two runs were run consecutively. The linear portion of the resulting graphs and data collected from the program were used to determine the modulus for our films.

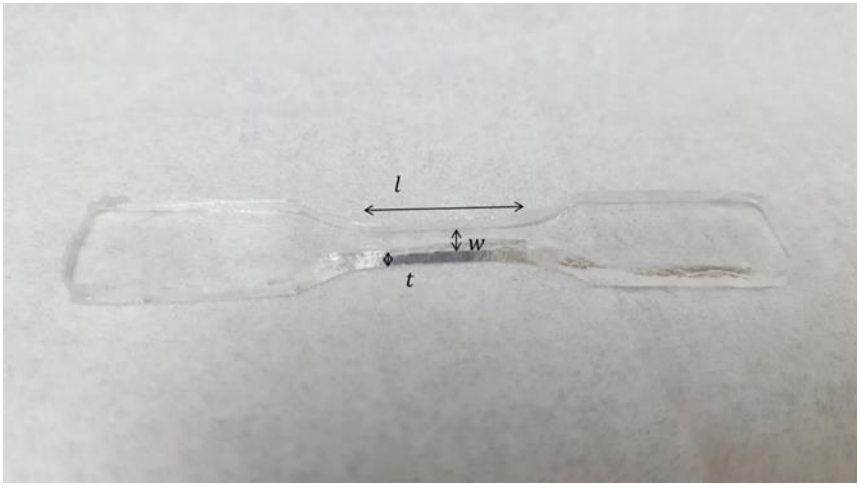

Figure 4. PDMS cut into a dogbone shape for ASTM tensile T-test to determine Young's modulus for 10:1 Slygard 184 film. Measurements taken were thickness, length, and width of narrow portion.

Results and Discussion

In a typical PDMS single bend experiment the advancing and receding force curves aligned in a predictable pattern without hysteresis, if the films were not experiencing fracture. Varying thicknesses of 10:1 PDMS films were bent; in particular PDMS films between ~0.2 mm to ~3.5 mm thick were measured. Film thickness was limited by the apparatus scale which could

not measure above 600 g when the bottom plate was present (~164 g) the scale could not measure below -27.8 g with bottom plate absent. Typical PDMS single bending force vs plate distance data for a thicker film (1.64 mm) is shown in Figure 5. The graph shows the forces both as the plate distance is decreased in bending from initial plate distance and as the plate distance is increased back to the initial distance.

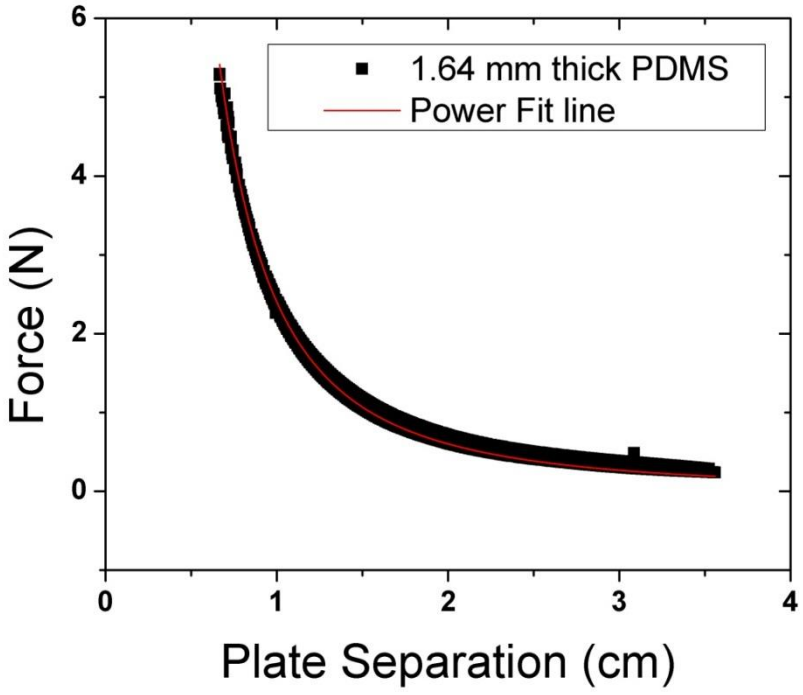

Figure 5. A typical force-separation curve for a PDMS sample of dimensions: length 79.93 mm, width 75.93 mm, and thickness 1.64 mm in the single bend geometry. Note the lack of hysteresis as the curve shows both advancing and receding data. The power law fit equation for this graph is $y = 2.4x^{-2}$.

The shape of the force vs plate distance curve was consistent for all thicknesses of PDMS examined, as can be seen in Figure 6. The closer the plates get to each other the higher the force and the smaller the radius of curvature of the bend in the film. Smaller radius bends experience more stress and force than larger radius bends for a particular thickness; this fits our

expectations, based on equation 11 and 12. Higher forces were seen for thicker films, even at larger plate distances, due to more material extending away from the neutral axis.

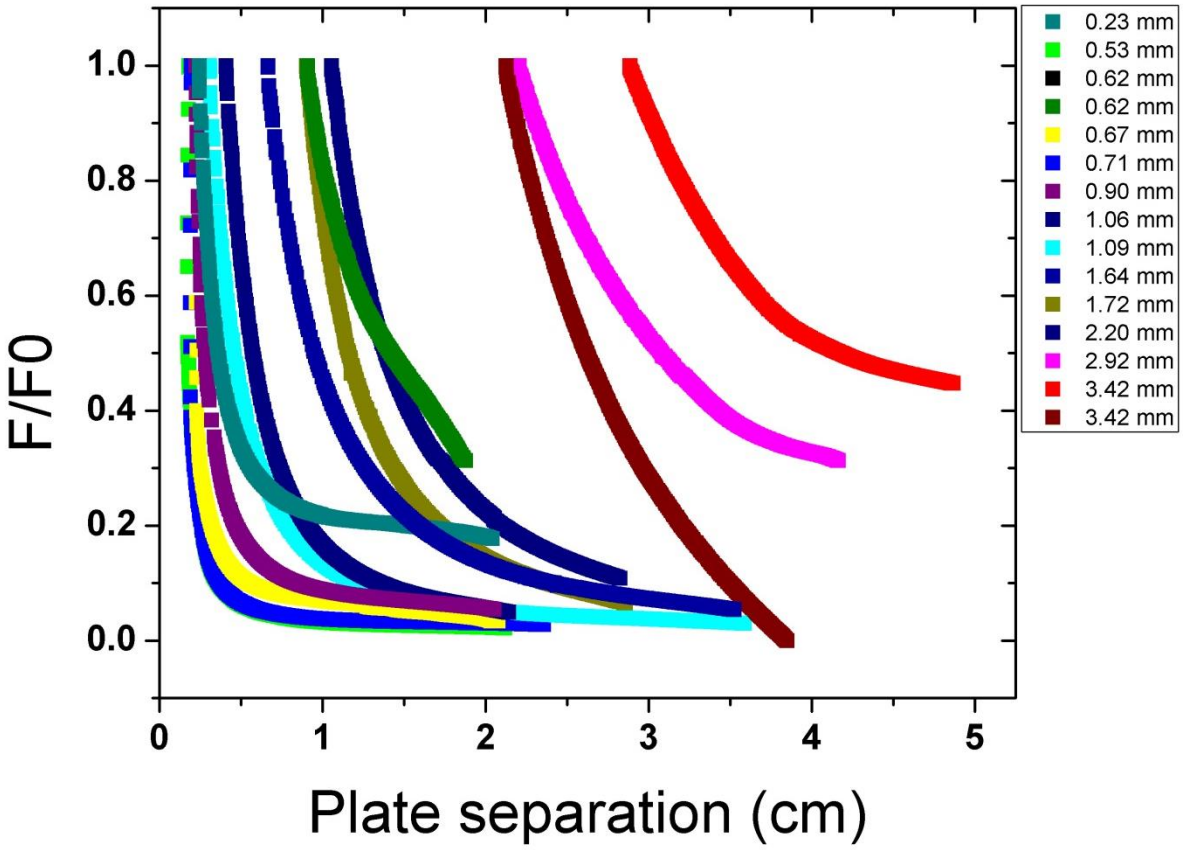

Figure 6. PDMS single bend compilation graph of films of thicknesses ≥ 0.23 mm.

PS films followed similar bending patterns as seen in Figure 7. In some cases there was no hysteresis evident. However, many bends showed hysteresis due to damage in the form of crazing or cracking. Generally as the plate distance and radius of curvature decreases the forces increase just like in PDMS. The increased thickness of PS led to increased stiffness that resisted bending for the small dimension of films used in our experiment, the thickest film bent was ~50 μm. The author bent films in the 10-50 μm range, thinner films were examined by other researchers in a parallel setup.

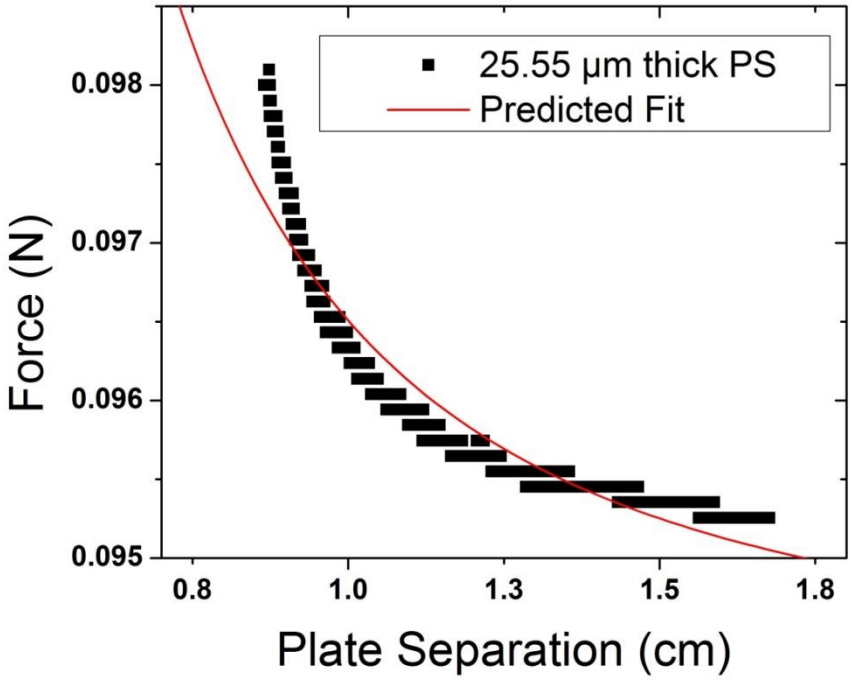

Figure 7. A force-separation curve for a PS sample of dimensions: length 39.88 mm, width 15.02 mm, and thickness 25.55 μm, in the single bend geometry. Note the lack of hysteresis as the curve shows both advancing and receding data, $y = 0.094 + 0.0023x^{-2}$.

All single bends of PS were compiled on a single graph, as shown in Figure 8. The force-separation curves of PS bends and thicknesses show similar behavior to PDMS with higher forces from smaller plate separation and smaller radius of bend curvature. There is a similar correlation between increased film thickness and increased force even at larger plate separation, as predicted from moment equations. Thinner films were less brittle and could sustain bending to higher curvature without crazing or cracking. PC films showed similar stress-strain behavior to the examined PS films in quasi-static single bends[76]. Thicker films even experienced clean breaks at force of 0.288 N for a film of 36.46 μm thickness and a plate separation of 0.267 cm. The peak pre-failure force for films in the thicknesses range examined here seemed to be ~0.3 N with plate distances between 2 and 3 mm.

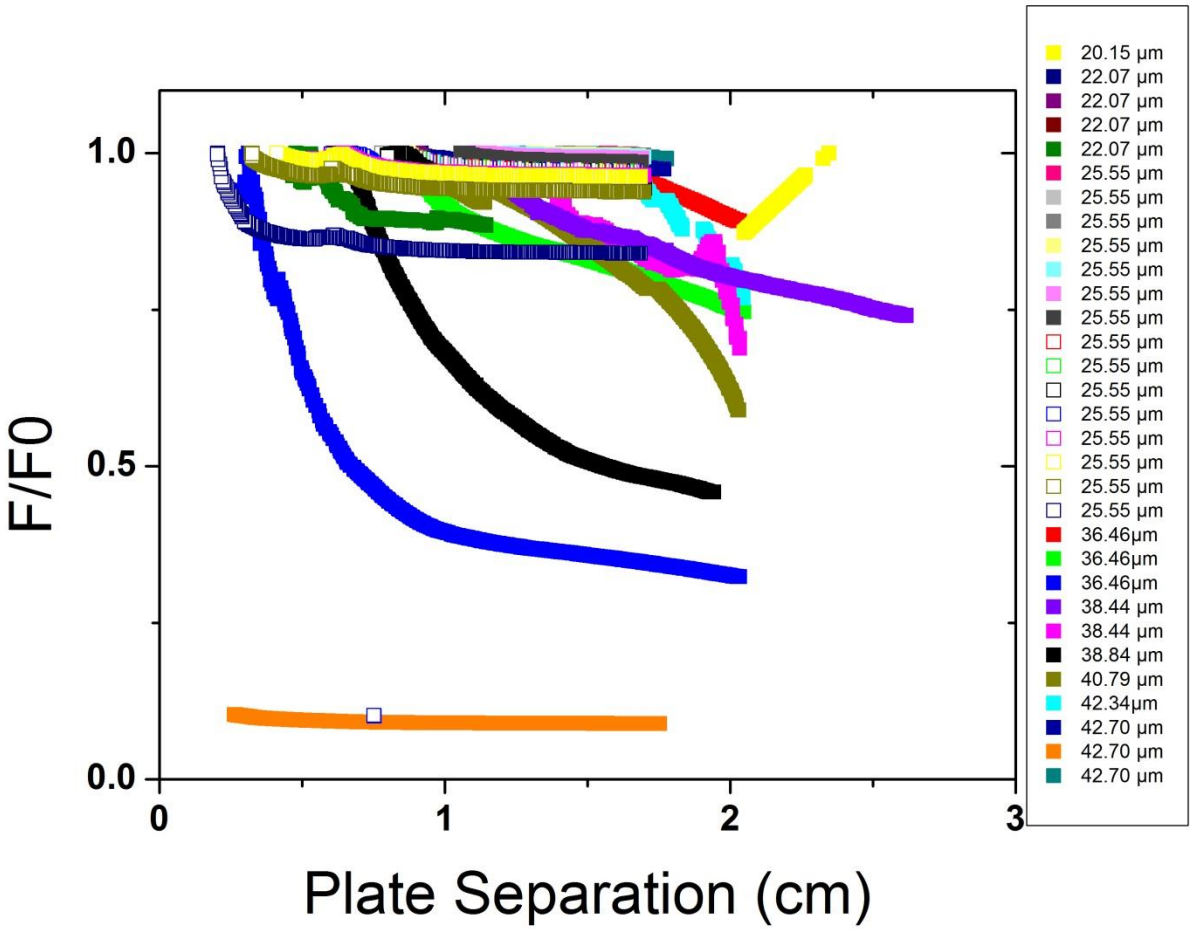

Figure 8. PS single bend compilation graph.

Equation 11 was fit to all force displacement data with only the bending modulus as a free parameter. All measured bending moduli were plotted on a log-log axis against film thickness in Figure 9. The data shows a clear cubic relation, as would be expected for a bending modulus. From the slope of a cubic fit the Young's modulus could be extracted. We found $E_{PDMS} = 1.6955 \times 10^6\, Pa$, which is in the range of the bulk modulus literature value 1.32-2.97 MPa[58]. The observed E_{PS} was also within literature values, 3-3.5 GPa[61]. PC with a modulus of 2.0-2.6 GPa[58] is also close as we observe the moduli of samples are close to those of PS.

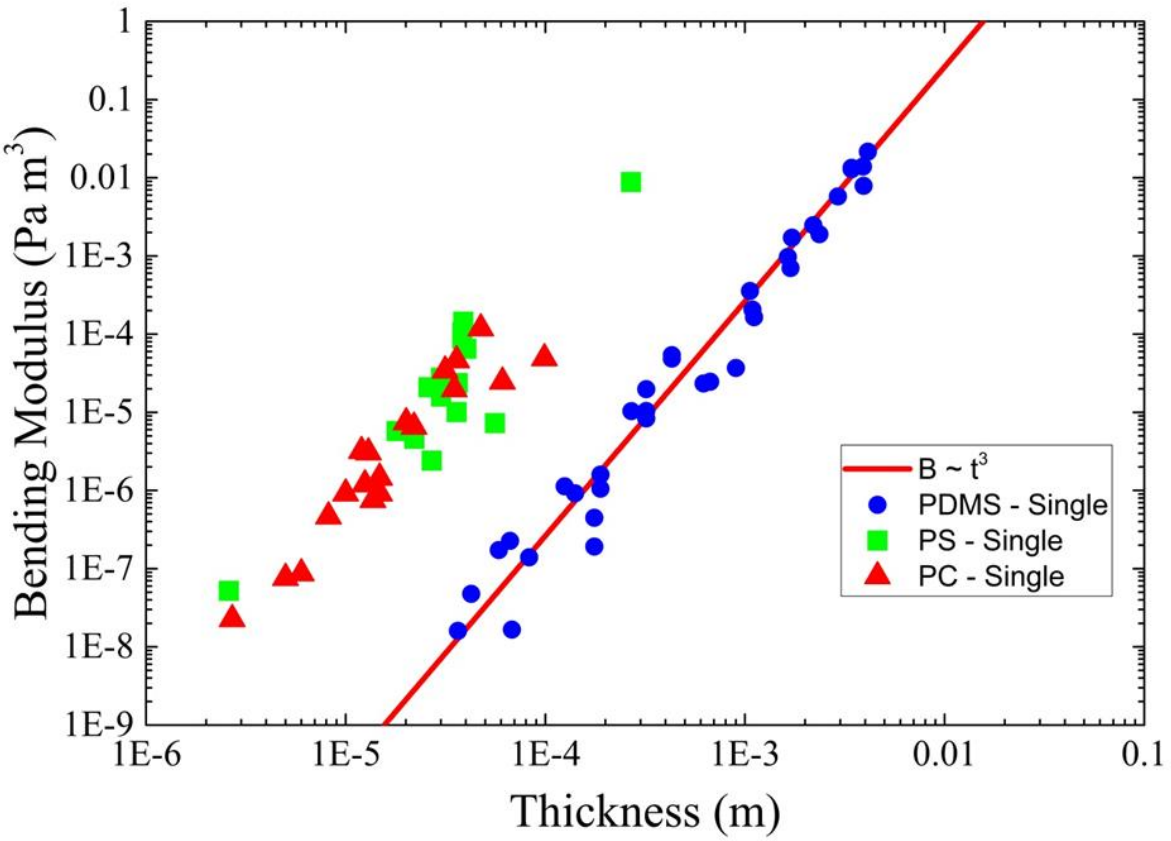

Figure 9. Compilation graph of all single bends of PDMS, PS, and PC fit to equation 12 predictions. The red line indicates modulus of PDMS as measured by tensile dogbone T-test. The prediction shows a good fit for our bending data. PC data collected by Dr. Andrew Croll.

The modulus of PDMS as noted previously is variable based on conditions of film fabrication, curing agent and curing temperature. To check our measurements of B we used a traditional test to measure the modulus of PDMS film. To determine the modulus of the films in our experiments four different thicknesses of a dogbone shaped PDMS sample were tested by a traditional bulk tensile test. The data from each test was graphed to determine the linear Hookean regime of each test (Figure 10). Thicker films had higher slopes than thinner films in force vs displacement, a trend seen in bending as well. The force vs displacement was then converted into stress vs strain which yields Young's modulus based on equation 5. The tensile

tests yielded a value of $E_{PDMS} = 1.1 \times 10^6 Pa$ which agrees well with our new experimental measurement.

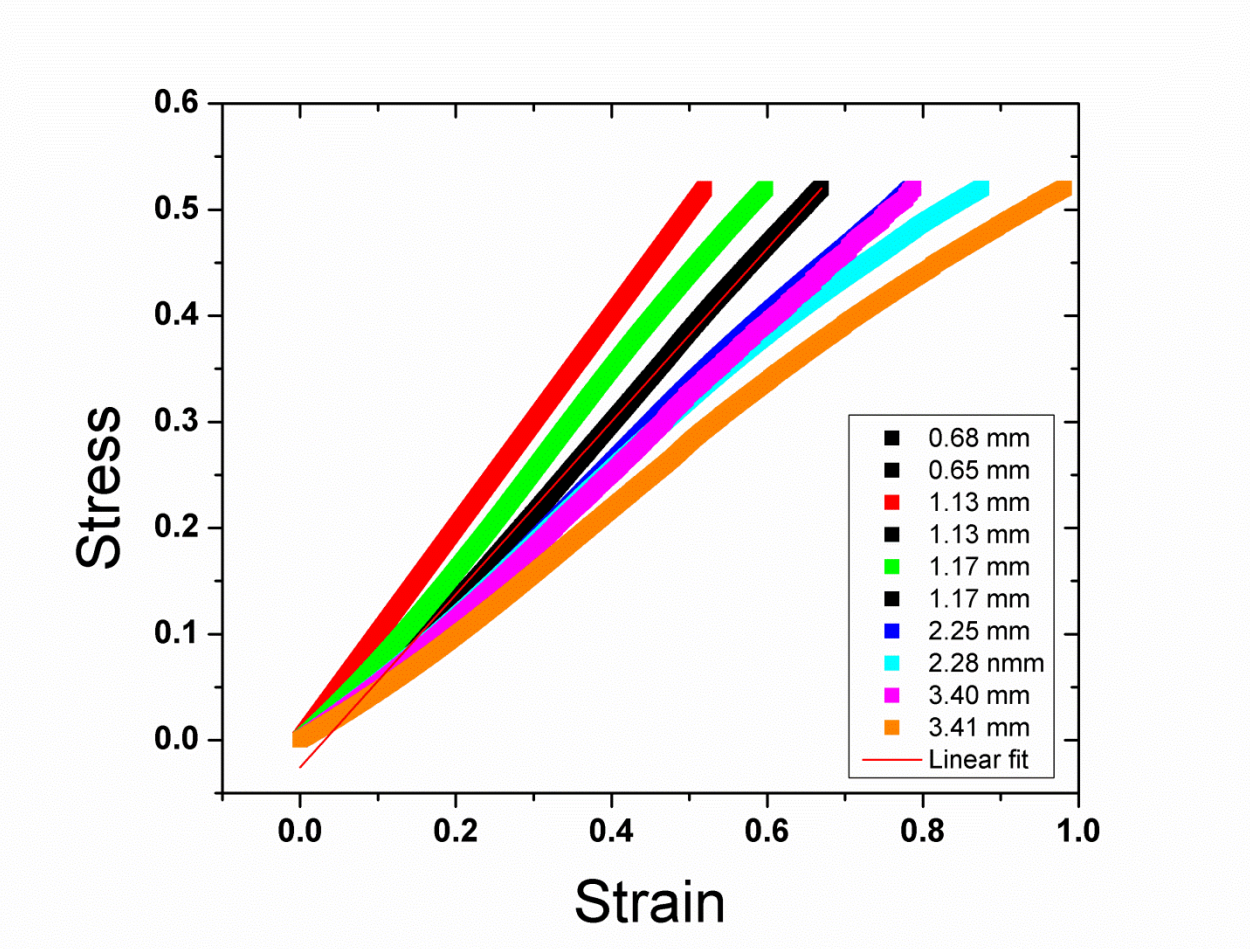

Figure 10. Linear regimes of dogbone tensile T-tests for four different thicknesses of 10:1 PDMS. Trendlines have slopes that all lay between $y = 8.31x10^5x$ and $y = 1.1 \times 10^6 x$.

The dynamics of single bends via force recovery were carried out on the same films, PDMS, PS, and PC[76], used in quasi-static single bending. Plates were moved together at constant speed until a desired force or displacement was reached. Plates were held in fixed position and force was measured as a function of time. Typical force recovery date from PDMS, sample is shown in Figure 11. It appears logarithmic, the predicted behavior of a viscoelastic solid[69]. This trend is seen on all samples of singly bent PDMS used in force recovery regardless of thickness (Figure 12).

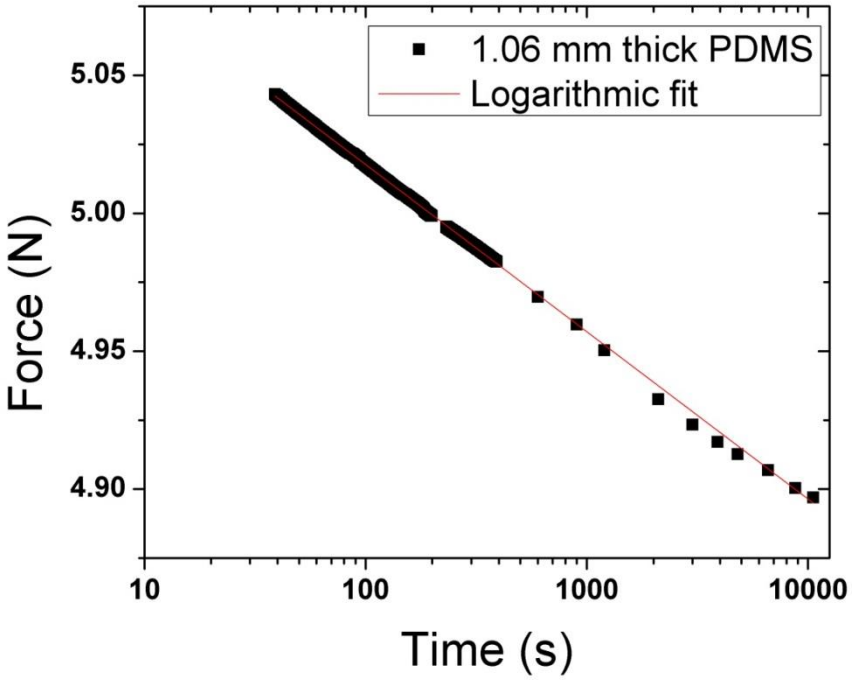

Figure 11. PDMS single bend force-time graph for a 1.06 mm thick film. The fit of a logarithmic trend $y = -0.060logx + 5.1$, (t)=$Alog(t/\tau)$, to the force decrease is shown.

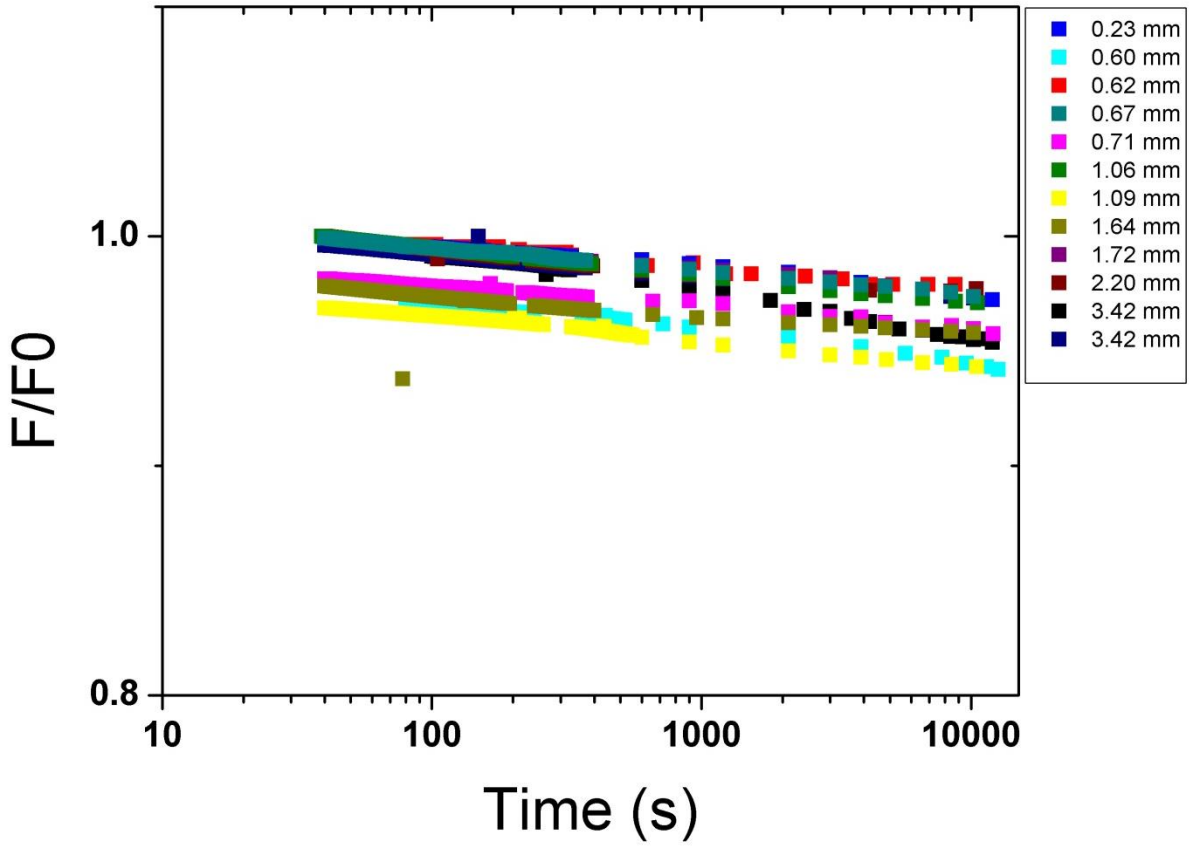

Figure 12. All samples of PDMS force recovery for single bends. There appears to be no difference in the response distinction based on film thickness.

PS when plotted on a force vs time graph does not show the logarithmic viscoelastic behavior of PDMS. The force decrease with time for PS fits a stretched exponential function as can be seen in Figure 13 and Figure 14. The behavior remained consistent with the different thicknesses in fit; however, the scale was more dependent on plate distance than thickness. This may be due to the scale of PS not being as large as that of PDMS which was from μm to mm in our bending, the thicknesses of PS only differed by tens of microns for all samples.

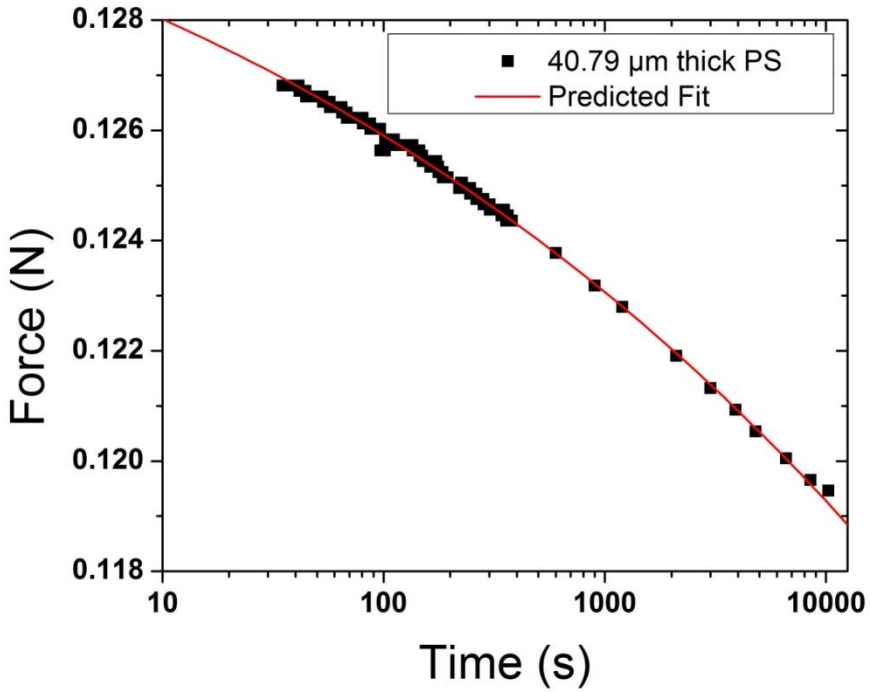

Figure 13. A PS force-time graph of a 41 μm film, one of the thickest to successfully bend. The fit for single bends lie along $(t) = -Aexp(-(t/\tau)^m)$ stretched exponential curves. Fitted to $y = 0.1339exp(-(x/6.94 \times 10^{10})^{0.1}$.

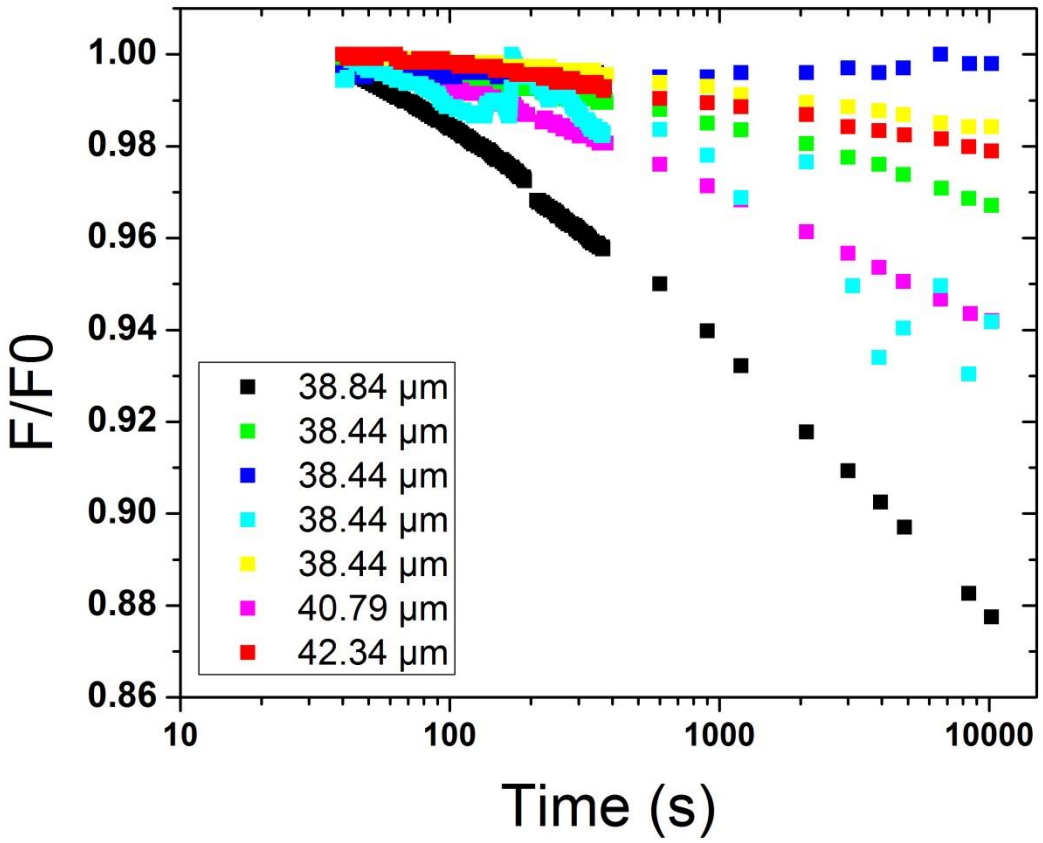

Figure 14. All samples of PS single bend of the films of thickness examined at different plate distances. Force decreases more quickly for smaller radius of curvature bends, those with smaller plate distances.

PC showed similar trends to those of PS in both quasi-static and dynamic single bends. The force-displacement of single bends of PC displayed the same exponential increase in force at lower plate separation as seen in PDMS and PS. In films where the PC did not sustain damage it bent reversibly with no hysteresis. In force recovery the Force-Time results were stretched exponential curves similar to PS[76].

Several researchers have studied the compliance of creep and relaxation in polymers such as PDMS and glassy polymers; however, they have used different methods to examine force recovery under specific conditions, such as temperature dependence[77], quenching time, and ultra-

thin scales. The methods differ from ours and include nanoindentation[78,79], laser interferometer[80], mechanical measurements such as stretching, tensile tests, and machine loading[81]. Other methods are often specific to thin or ultra-thin films including photobleaching[70], microbubble inflation[82], or dewetting[83]. Our approach has range and versatility not seen in many other methods that are limited to bulk or ultra-thin films. Our research fills a niche for polymer structure mechanics as most of the aforementioned do not take into account geometry of a material or the mechanics of the material in a specified geometry to determine unknown material properties.

Conclusion

Our experiment singly bent polymeric films, PDMS, PS, and PC, between two plates to determine engineering related properties. Films were bent quasi-statically in forward and reverse to examine force increase in relation to decreasing radius of bend curvature, thickness, and material properties. All three of the films experienced exponential increases of force with decreasing plate separation and corresponding decreases of force as plate separation increased. All films also showed higher forces with increased film thickness as predicted by moment equations. Hysteresis was only seen in samples experiencing some type of failure, cracking or creasing. Our findings also support that bending can be a reversible non-damaging process below the polymer's stress threshold.

Data from all of the films was then compiled together on a log-log graph of $B \sim t^3$ with E, Young's modulus as the only unknown parameter as it can differ depending on temperature and curing factors. This data fell nicely along lines with a slope of E for each material respectively. We then compared the attained moduli of PDMS from our bends to moduli attained from another

test, a classical tensile test. The tensile test modulus agreed well with our bending modulus. Bending presents a valid method for determination of a material's modulus.

In order to further examine the mechanics of the materials in the single bend structure we then carried out force recovery. The force recovery of PDMS differed from that of PS and PC. PDMS had logarithmic force-time decrease while PS and PC exhibited stretched exponential behavior; the force decrease was much faster for the glassy polymers than it was for PDMS. PDMS force recovery was consistent across the large range of samples tested. PC differed with plate separation and initial force.

Our findings on the behavior of materials in bending, to different radii of curvature and with respect to time, improve understanding of the mechanics between structure and the model materials examined. We have also demonstrated that modulus can be determined through a method of film bending. The trends noted from our bendings, dynamic and quasi-static, aid in understanding of polymeric film mechanics and engineering.

CHAPTER 2. BENDING AND FORCE RECOVERY OF D-CONE IN POLYMER FILMS

Background

Origami patterns and crumpled balls often hold their shape due to sharp bends, creases, or stretching in the thin film they are constructed with. The pointed nose on a paper air plane is a structure that is engineered to achieve a certain objective; in the case of the airplane it is to increase aerodynamic properties. This corner or point of a paper airplane is an example of a developable cone (D-cone). A D-cone is a conical shaped point region of film where stretching has been localized into a singular point. The singular point is surrounded by non-stretched areas in the film even though the film may contain bends. The D-cone is a localized area of strain in a system[84]. The energy that is needed to stretch a system is larger than the energy needed to bend a system in thin elastic sheets[85]. This is why in order to conserve energy the material stretches the smallest area it can, effectively a single point. In our work we investigated the effects of D-cones on film mechanics by doubly bending a thin film.

Stress-strain behavior of a system is the result of the combination of its geometry and material properties. Four main quantities noted for engineering polymer based materials are: modulus, ultimate elongation, elastic elongation, and tensile strength, the stress required to achieve failure[3], which are all specific stress-strain considerations. Doubly folded films are tested under compression. With the system in double bend geometry, a natural next step is to observe this stress-strain behavior with respect to time in force recovery measurements. Failure, such as cracks, along the bend, is also an undesirable occurrence as it is an example of energy localization outside of the D-cone geometry.

Experiments looking into D-cone formation and the effects this may have on a material have been carried out on thin elastic plates[86], shells[85] and papers[84], however, there is a lack of

information connecting the D-cone to specific material properties. Our experiment examines polymeric systems to see if they form D-cones and what affect this geometry has on the stress-strain response of the system in bending of doubly folded films.

Theory

Stretching is localized in a D-cone so the stretching energy of the surrounding system is not considered important to the total energy of a thin film with a single D-cone in it. In a thin film the stretching energy is:

$$U_s \approx E_s \gamma^2 \Delta S \quad (13)$$

where E_s is stretching stiffness, γ is the in plane strain, and ΔS is the area of the stretched region. The energy stored in the bending needed to create the D-cone singularity is:

$$U_b \approx E_b \kappa^2 \Delta S \quad (14)$$

where E_b is bending modulus and κ is the mean curvature in the D-cone core[87]. The core refers specifically to the small region near the tip of a D-cone that experiences stretching[88]. The core region has a mean curvature κ which is: $\kappa = \frac{1}{R_c}$, where R_c is the radius of the developable cone in the core region close to the tip.

The size of the core region can then be determined through a scaling argument constructed by equating the energy from stretching and energy from bending. The result is a power law:

$$R_c \approx \left(\frac{E_b}{E_s}\right)^{1/6} \Phi^{-1/3} {R_s}^{2/3} \quad (15)$$

where Φ is the angle of the 'cone' shape formed by the sheet and R_s is the sheet. For an isotropic, homogenous, material:

$$\frac{E_b}{E_s} \approx {t^2}/{(1-v^2)} \quad (16)$$

where t is thickness of the system and v is Poisson's ratio for the material[84]. We note the weak dependence on the opening angle of the cone is the only connection to the boundaries in which the cone has been formed.

Experiment

The experimental setup is the same as in chapter 1 with the only difference being that the films are doubly bent and not singly bent. To double bend a film, the film is folded along its longest side, and then is bent along the new longest side. The film is then placed in apparatus with double bend section of the film facing the camera in order to observe D-cone formation. All other aspects remained the same as for a single bend.

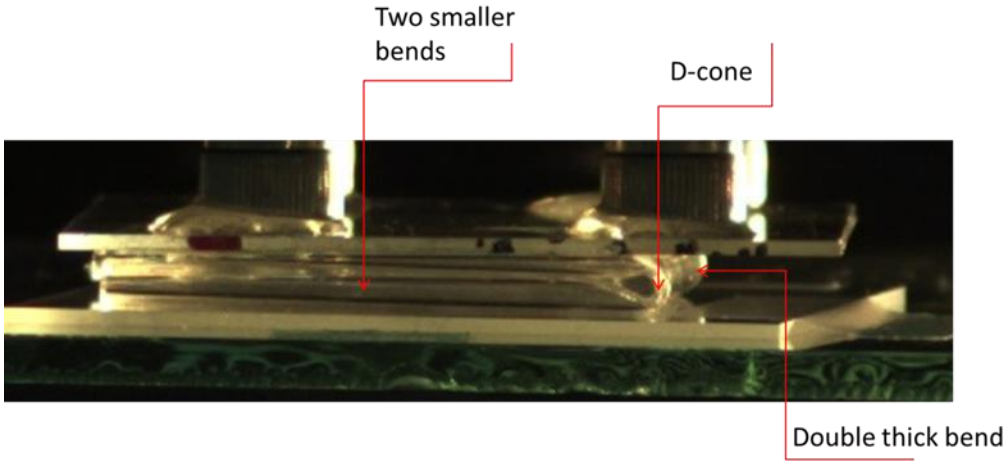

Figure 15. A doubly bent film of 0.67 mm thick PDMS between two plates with D-cone formed.

Videos and pictures were taken in short regular durations. Limited by software lag times between 10 and 40 seconds two videos were taken back to back, also separated by lag time. The final procedure for force recovery was two videos with pictures taken at short time intervals followed by pictures taken 10 min, 15min, 20min, 35min, 50min, 65min, 80min, 110min,

140min, and 170 min from start time. This progression of longer time intervals was due to the logarithmic nature of force recovery stated in background.

The double bends were carried out on the same films used in single bendings: PDMS, PS, and PC of varying thickness. The author created PDMS thicknesses: ranging from 0.23 mm to 3.43 mm and PS thickness: 10 μm +. Data from thinner films were collected by Dr. Andrew Croll, on a parallel miniature setup and data on the present setup was also collected by Dr. Damith Rozairo. PDMS films could be bent multiple times due to their elastic nature while PC and PS were limited to a single bend experiment due to their low failure threshold.

Results and Discussion

PDMS films of varying thicknesses were doubly bent quasi-statically in our apparatus. The force-separation curves showed no hysteresis unless damage occurred which permanently creased the film, an occurrence that was limited to thin films at small plate distances and high radius of curvature. The force-separation curves of doubly bent PDMS films followed power law, Figure 16, similarly to singly bent PDMS films. The compilation of double bends shown in Figure 17 is also similar to that of single bends. There was alignment of each thickness along its respective force-distance curve even when multiple bends were done on the film on different days or in succession. Thickness was the dominant factor in determining the overall force peak. The formation of a D-cone did not appreciably change the double bending behavior in comparison to single bending behavior. As in single bends experiments, films beyond a certain thickness could not be observed in our apparatus due to forces being too high for the scale.

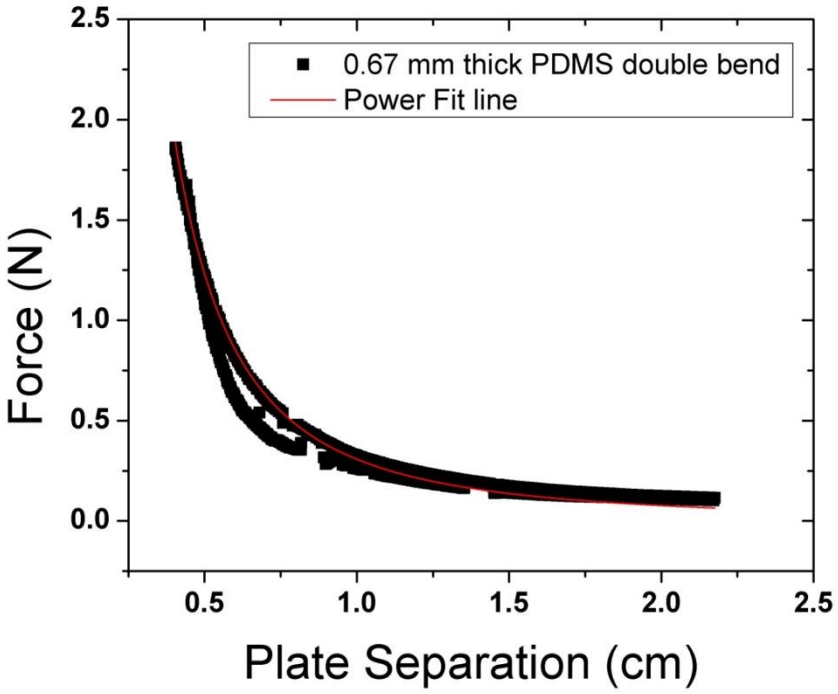

Figure 16. A typical force-separation curve for a doubly bent 10:1 PDMS sample of dimensions length 79.62 mm, width 73.05 mm, and thickness 0.67 mm in the single bend geometry. Note the lack of appreciable hysteresis as the curve shows both advancing and receding. The power law fit equation for this graph is $y = 0.29x^{-2}$.

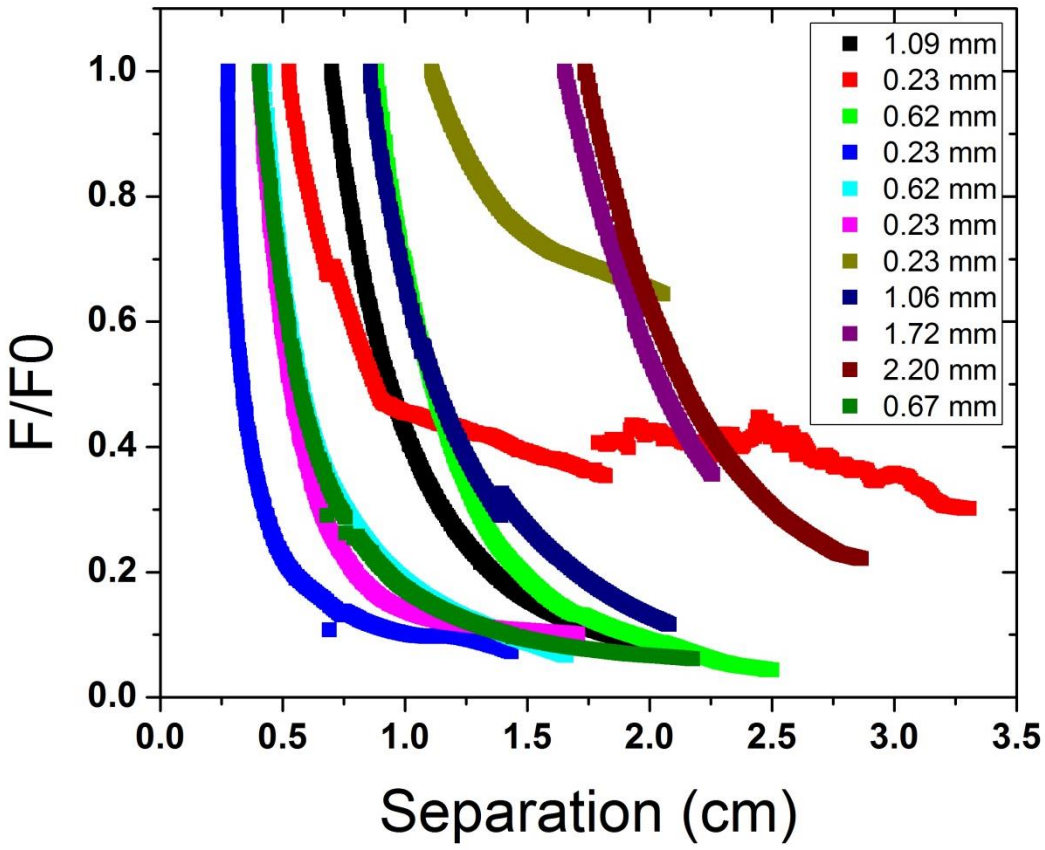

Figure 17. PDMS double bend compilation graph of films ≥ 0.23 mm thickness. Force has been normalized.

There is less data for PS double bends as at the thicknesses examined damage tended to occur during the process of folding and placement into the apparatus. The double bend of the film carried out by the author did not have a semicircular bend while in apparatus it was more square and angular (suggesting some degree of damage). Thinner films were less likely to break during experimental preparation. Unlike PDMS the double bends conducted on PS always showed appreciable hysteresis even at smaller compression distances, shown in Figure 18. However, bending of the same thickness did lie along the same force distance curve as shown in Figure 19, when plate distance was decreased successively. Force remained fairly constant for large bending curvature and increased sharply only when a certain plate distance and radius of bending curvature were reached.

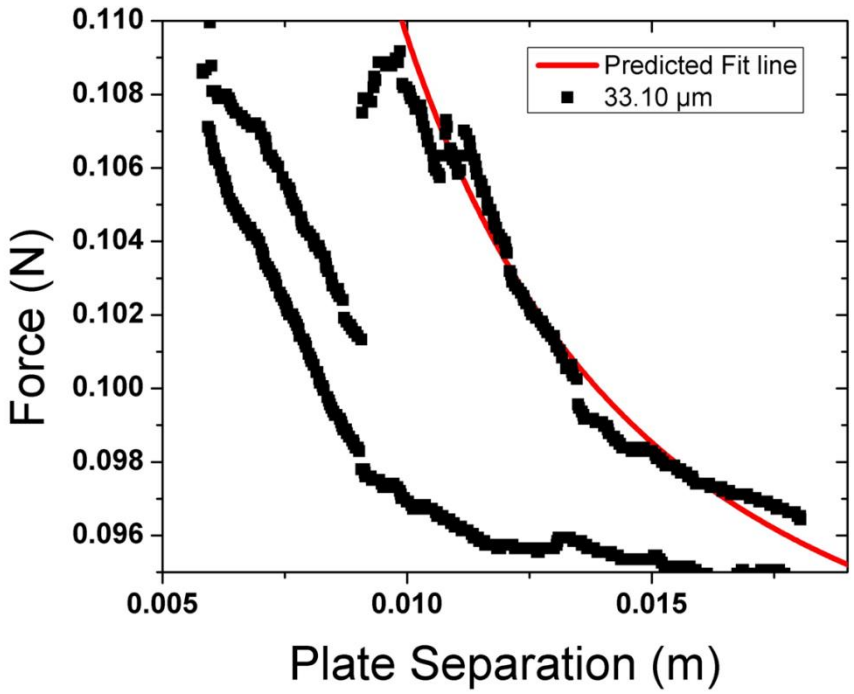

Figure 18. A force-separation curve for a doubly bent PS sample of dimensions length 43.5 mm, width 20.54 mm, and thickness 33.10 μm. Note the hysteresis as the curve shows between advancing and receding data. Fit curve is $y = 1.99 \times 10^{-6} + 0.090x^2$.

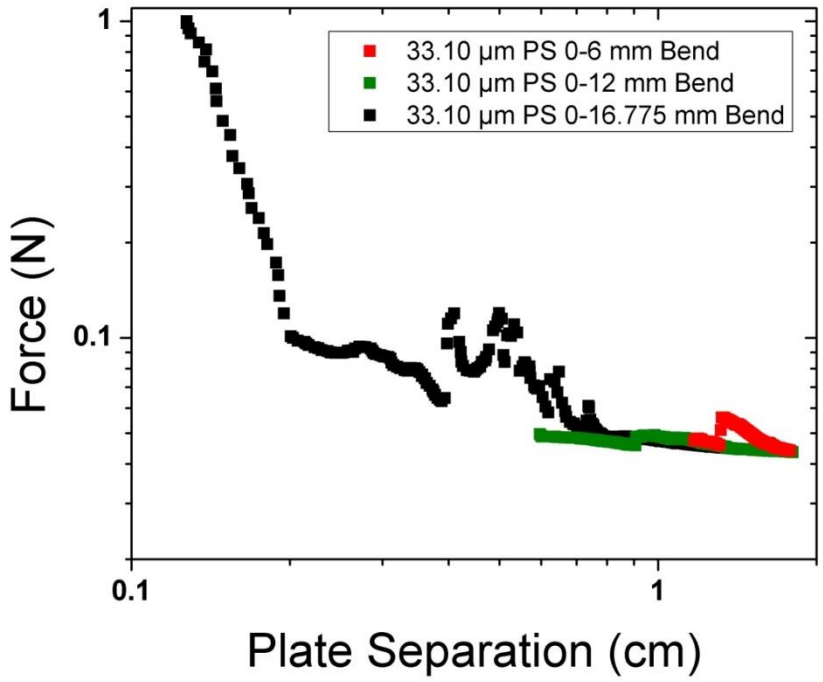

Figure 19. Three consecutive bends of a PS film to decreased plate separation. PS film was of dimensions length 43.5 mm, width 20.54 mm, and thickness 33.10 μm in double bend geometry.

Two assumptions were made in order to interpret the force displacement curves for the double bends. The first assumption was that the D-cone did not contribute to the strength of the structure. The result of this assumption is that the structure only contains two bent regions of film. Without the D-cone equation 12 is therefore valid for fitting the data. The second assumption is that since thickness was twice as large the dominant energy of the system is from the doubly thick bent region (where the film overlaps itself).

The resulting measurement of B was then plotted in Figure 20 against the modulus found from single bend data. The fit for doubly bent films was nearly identical to that of singly bent films in falling on the same $B \sim t^3$ line. This strongly supports our assumption that the energy of the D-cone did not significantly change the system compaction and can thus be ignored.

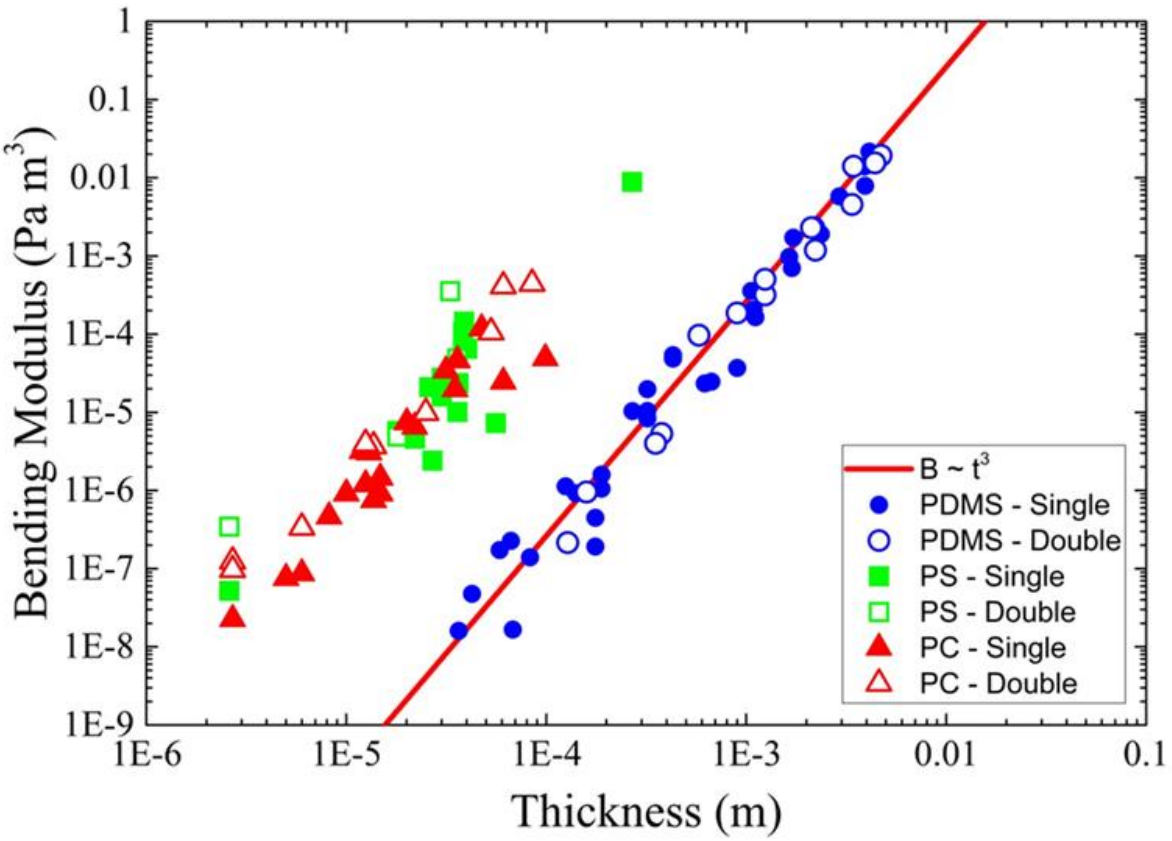

Figure 20. Bending modulus-thickness plot of all double and single film bends on log-log plot. All bends lie on the line of increasing bending modulus with increasing thickness.

The D-cone absorbed the strain from the folding and the bend by localizing it in a small stretched region[84]. Bending forces are predominating in the rest of the film as it does not stretch. PDMS film stretching was reversible while for PS and PC[76] it resulted in permanent damage, cracks and deformation respectively. Despite the damage, the D-cone present in the doubly bent films DOES NOT contribute to its load bearing ability, rather it provides a mechanism for the release of the strain built up in the film via deformation. The D-cone does not contribute to the load bearing ability of a doubly bent film because it is not significantly changed during subsequent deformation.

Force recovery showed differing trends between the filled elastomer and the two glassy films. Graphs of double bend force recovery data for PDMS is shown in Figures 21, and PS is

shown in Figure 22. Figure 21 depicts the force vs. time graph of a 1.72 mm PDMS film, in the middle of our thickness range. The trend line fit is logarithmic with only slight deviation; the stress of the film decreases proportionally on scales of time ten times as large as the previous length of time. The PS force recovery graph for a 33.10 μm film, in the middle of the thickness range of those bent by the author and shows a stretched exponential fit. The stretched exponential shows force decrease is initially slow with the amount of change increasing on the logarithmic axis. The PC force recovery is similar to the PS film force recovery and has a best fit to a stretched exponential function. There is more variance with the PC data however as it seems to have wider variation at longer time scales[76].

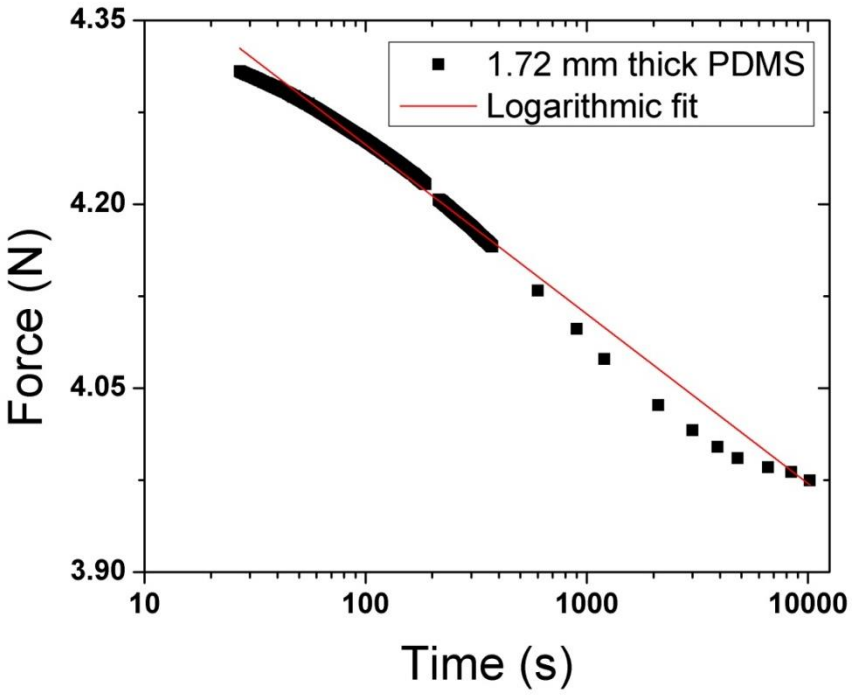

Figure 21. PDMS force-time graph for a 1.72 mm thick film doubly bent with pre-double bend dimensions of 80.15 mm length and 75.77 mm width. The fit for the double and single bends is logarithmic $(t)=Alog(t/\tau)$, $y = -0.060logx + 5.138$.

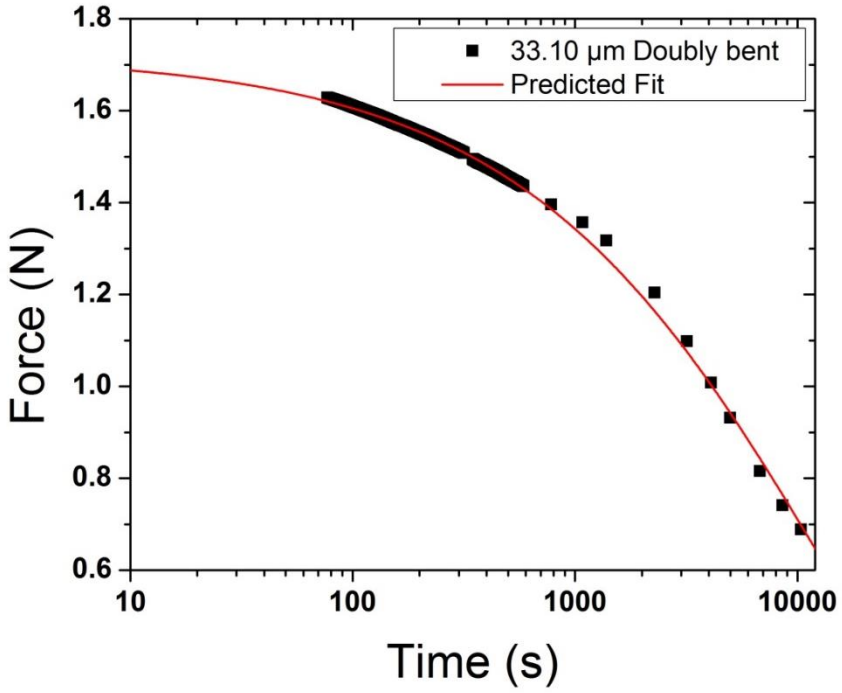

Figure 22. A PS force vs. time graph of a 33.10 µm film with pre-bend length of 43.5 mm and width of 20.54 mm. The fit for the double and single bends lies along a $y = 1.72\, exp\left(-\left({}^{x}/_{12500}\right)^{0.55}\right)$ stretched exponential curve.

All of the doubly bent and singly bent samples for force recovery data were then compiled onto single graphs; force recovery of PDMS is shown in Figure 23 and force recovery of PS in Figure 24. All thicknesses of PDMS displayed the same trend after normalization by the force measured at 40 seconds. The differences in the force recovery behavior of PS can be attributed to initial plate separation and initial force. Smaller plate separation and higher initial force had more rapid decrease in force with respect to time. This means that we saw a more rapid decrease in force at smaller bending radius of curvatures. PC force recovery was carried out for a range of thicknesses. The PC response was similar to that of PS[76].

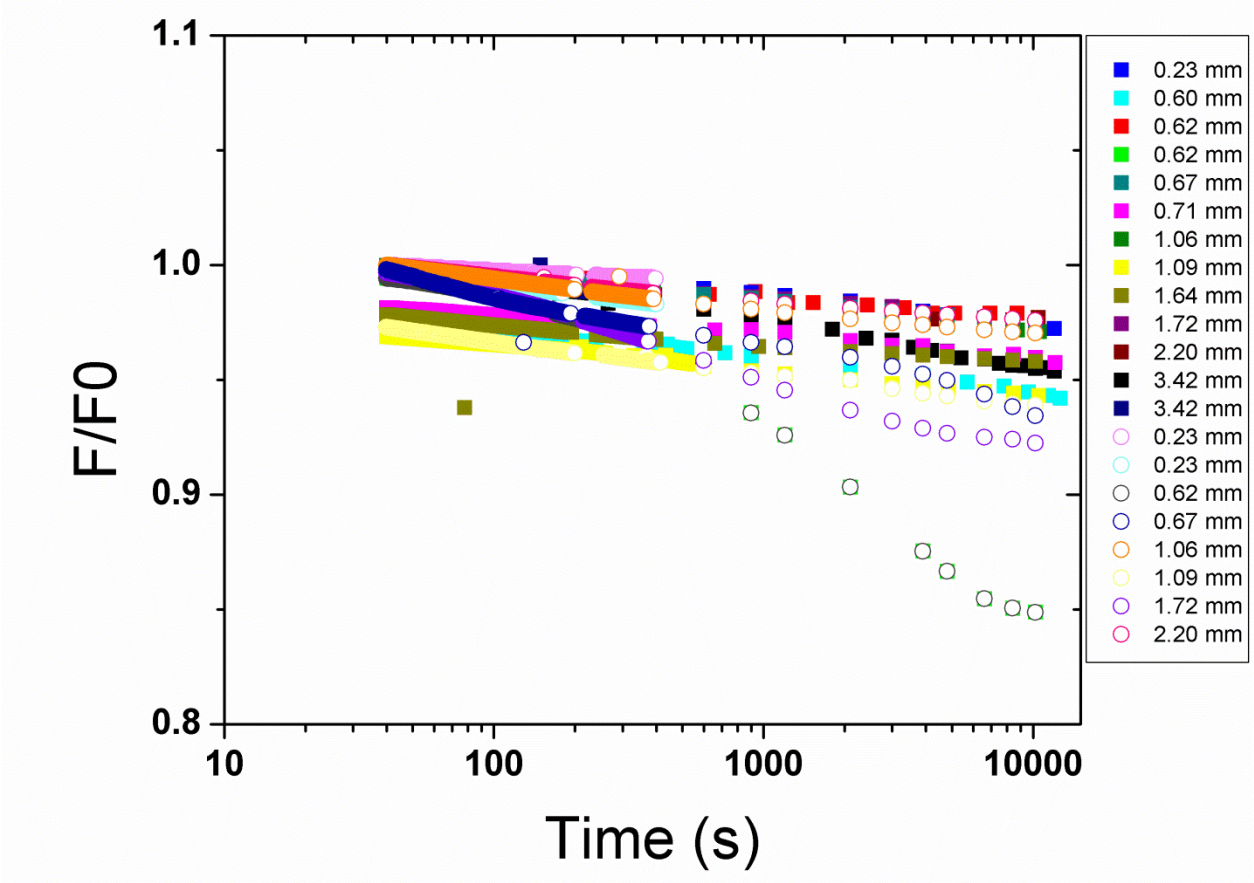

Figure 23. All samples of PDMS force recovery for single and double bends, normalized. There is no response distinction between the single bends and double bends or between thicknesses.

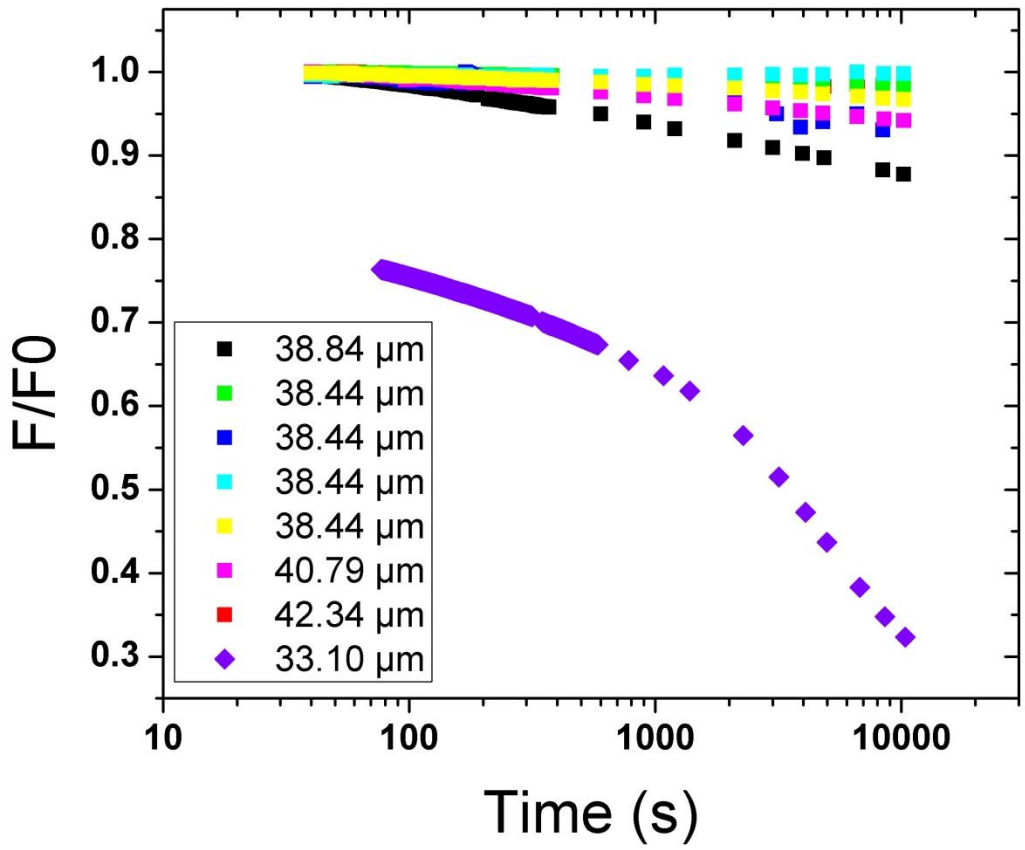

Figure 24. All samples of PS single bend of the films ~40 µm thickness at different plate distances. Force decreases more quickly for smaller radius bends.

The results for double bends are the same as corresponding single bend force recovery. PDMS had a slower force recovery than PC and PS. PDMS force recovery, as can be seen in Figure 23 was not dependent on film thickness with most of the normalized curves overlapping in similar logarithmic curves. Meaning the decrease in stress was not significantly larger in the thicker films, therefore, the force recovery behavior is more a product of the material than of the bending radius of curvature and thickness.

PC and PS force recovery showed stretched exponential function trends. The glassy films recovered more quickly than PDMS with a rate dependent on strain as the glass evolved increasing surface strain from higher bending curvature, especially notable in Figure 10 for PS. PS and PC recovered more quickly at different rates. The speed of force recovery was possibly

due to relaxation mechanisms of the amorphous molecules rearranging. The force recovery of singly and doubly bent films exhibits the same behaviors for all three films in comparison to single bends.

All three types of film experienced failure at high loads or following aging. Thinner films of PDMS experienced permanent creasing under large constant loads and small plate distances. Older PDMS films that had been subjected to force recovery numerous times and asymmetric films also experienced fracture failures. PS cracked under too high of loads with damage in the form of crazing or fracture breaking the film cleanly in half in some instances. When PS cracked before the final displacement and load was reached, in some instances cracks increased when left overnight. These failing samples were excluded from data as they had other factors that altered the strain distribution under stress.

Conclusion

Our experiment aimed to increase the literature and understanding of the effect of D-cones in polymeric materials (PDMS, PC, PS) on their stress-strain response and how the systems recovered over time at constant loads. We created doubly bent films and carried out force-displacement compression testing in the same manner as the singly bent films described in chapter 1. Data was fit with predictions in order to determine differences. No differences were observed leading to the conclusion that the D-cone is not load bearing and does not affect compaction. Force recovery was then carried out on the three polymeric systems in double bend geometries when applicable. PDMS recovered logarithmically while PS and PC[76] recovered much faster in a stretched exponential fashion possibly accounted for by molecular arrangement. The D-cone did not contribute noticeably to force recovery as double bend and single bend samples of PDMS exhibited similar force recovery curves. Future work remaining to be done is

expansion on the stress-strain behavior of the thicker glassy films though single bends, double bends, and force recovery and more specifications of the D-cone geometry for each of the model materials.

CHAPTER 3. MICROGEL PARTICLES FROM TRIBLOCK COPOLYMER PS-PAA-PS

Background

Microgel particles and nanogel particles are smart responsive materials used currently in pharmaceuticals as capsules for drug delivery[89,90], medical imaging[91], coatings, printing applications[89], pollution control systems, catalysis[90], food engineering, cosmetics[92], and personal care products[91]. Microgels are defined as micro or nanoscale cross-linked latex particles[89] or colloidal polymer networks which encase a solvent[93] in a polymer mesh and respond to external stimuli such as temperature, pH, magnetism, electrical fields, salt, light, ultrasound, and solvent chemistry[94]. Microgel particles have combined polymer and colloid chemistry, properties, and physics. The flexible nature of microgels make them able to compress and pack together in high densities[89,91,95]. The potential exists for expanding the applications of these structures into other uses and expanding their abilities in current usage through tuning environmental responsiveness and structure complexity[89,93,96,97].

Gels are 3D macroscopic networks of connected molecular subunits that have non-zero shear modulus, are structurally disordered and may contain high liquid volume fractions of solvent. Macroscopic properties of gels change based on the number of bonds and type of bonds between molecules which can be chemical or physical with physically bonded gels being thermoreversible[98]. Mechanical properties can be improved in macrogels through modifications of architecture or the addition of inorganic particles incorporated into the gel matrix adding additional response ability to stimuli such as electricity and magnetism. However, there are many clear advantages to microgel particles. Microgel particles have been found to swell much faster than macrogels by as much as eight orders of magnitude[99] and have higher exchange rate at the surface; a property useful in drug delivery applications along with the biotechnology

advantages of colloids[100]. Microgel particles have the advantages of gels, such as high solvent absorbance, yield stress[89], and softness, without some of the disadvantages: hysteresis in transition between swollen and non-swollen states, irreversible expansion or compression, and slow absorbance or diffusion rates. In macrogels liquid taken in results in tension, the fluid is released under compression[101] force; microgel particles do not release their solvent under compression; they are softer and more deformable. Microgels are able to squeeze through small spaces, and undergo changes in volume under stress[102] without sustaining the damage[91] that a macroscale hydrogel would[103]. The mechanical properties are sometimes large enough to be measurable through micropipette aspiration where a micropipette is used to aspirate a particle into a micropipette. The deformation and suction force provide information on particle elasticity, and possible lysis points[104]. Microgels have lower viscosity within the same occupied space compared to hard sphere particles, have high water/solvent content, elasticity, and the high surface area to volume ratio of a colloidal particle[89]. Generally below micrometer size diameters microgels remain colloidal and do not precipitate out of solution even during swelling, subject only to Brownian diffusion from thermal energy[101].

One of the biggest advantages of microgel particles is their swelling from external stimuli, the polymers of the particle expand outward and the particle enlarges, changing the dimensions of a particle reversibly (Figure 25). Changes in size and other microgel properties lead to behavior and properties that differ from that of traditional hard sphere particles and colloidal systems[91,105]. Swelling is influenced by osmotic pressure differentials between the external polymer segments, those interacting with surrounding solvent and internal polymer segments in microgel interior. During expansion previously buried regions are exposed[97] in substantial numbers, these newly exposed polymer regions can interact with the surrounding

external solvent providing possibilities for functionalized monomer attachment[89]. Good solvents induce swelling while bad solvents lead to compaction[89,91,106]. Swelling and collapsing can be tuned either through physical changes, polymer composition, or chemistry of the particle or solvent. Optical properties also change as particles swell; the enlarged particles approach index of the solvent and the deswelled particles are close to the index of the polymer. Certain microgels such as PNIPAM, can crystallize into exotic arrays further affecting Bragg scattering in both crystal form and melting[91,107,108,109]. Multiple stimuli may not contribute to swelling additively.

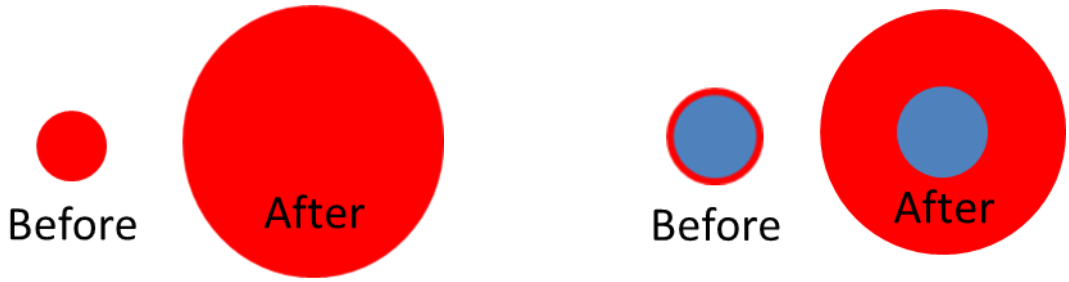

Figure 25. A general schematic of particle swelling. Before indicates a particle in an unswelled state and after indicates a solvent swollen particle. The left pair shows a standard microgel particle. Swelling of phase separated amphiphilic block copolymer particle is shown in the right pair of images. Blue is the core block and red is the outer solvent responsive block which collapses in bad solvents, before, and swells in good solvents, after.

Microgel particles have predictable behaviors based on the polymer composition of the mesh and the solvents they are interacting with. Solvents that cause swelling expansion of the microgel particle are known as good solvents while those that lead to the particle collapsing inward are known as bad solvents[97]. The degree of swelling and deswelling describe the size range of a microgel particle which impacts the possible uses of the particle[89]. This allows for taking advantage of chemistry such as surface functionalization: immobilization, tracers, transport, delivery, structural support, recognition, sensors, surface modification such as hairy particles or those with hydrophilic or hydrophobic layers or areas, rheological effects, or

saccharine coverage[110]. Proteins for transport and biomineralization, can be complexed into the structure to add functionality and stability[104].

Microgel particles are versatile due to their deformability and can be of use in emulsions and foams which maintain high surface tensions[111,112]. Concentration can be increased with volume fractions close to 1, forming pastes[113,114] due to a unique relationship between volume fraction and polymer size[89]. Hard particles exhibit characteristic rheology of increased viscosity with increased particle volume fraction[115]. Increased volume fraction of crosslinked polymeric nanoparticles, however, exhibit the opposite rheology, high volume fractions have decreasing viscosity (shear thinning) attributable to increased free volume and improved energy dissipation[116]. The particles can also be used to co-assemble other nanoparticles from inorganic constituents due to the ability for smaller particles and polymers to pass through the polymer mesh shells[117,118,119]. The inclusion of smaller particles and polymers can affect the osmotic pressure balance or solvent-particle interactions[89].

The first reported microgel particles were crosslinked divinylbenzene (DVB) of narrow size dispersion synthesized in 1935 by Staudinger and Husemann[89]. Since 1935 numerous other polymers have been found to effectively form microgel particles such as polystyrene (PS), and poly(N-isopropylacrylamide) (PNIPAM). In certain polymers such as polyacrylic acid (PAA), pH can stimulate swelling via a reversible proton exchange with solvent/water from a pendent group that is either acidic or basic[101]. The electrostatic interactions from charged groups increase inherent stability[89] even as they swell. This aligns with other studies where small changes can have large effects in microgel particle outcomes[120]. Addition of excess electrolytic polymer such as PAA to microgel solutions had lowered osmotic pressure and deswelling effects; when PAA was also a component of the microgel particles swelling occurred at higher pH values. Charged

groups along polymer backbone affect microgel stability and osmotic pressure stabilizations[89,97]. Addition of polyelectrolytes, therefore, gives additional functionality and versatility to microgel particle systems[89] including responsive polymer conjugates for biological molecules such as antibodies and enzymes[94].

Microgel particles can be formed in several ways, all of which follow one of two general pathways: disintegration of larger structures through breaking of interparticle bonds or aggregation in high solution concentrations, promoting noncovalent interactions[104]. The most common methods of microgel synthesis are the result of direct synthesis emulsion polymerization[121,122], anionic polymerization[123], inverse micro-emulsions polymerization[89,124] followed by cross-linking of the polymer chain[125] often through photo catalysis, and heterogeneous polymerization with bifunctional or multifunctional cross-linkers[126,127], and self-assembly via kinetic channels. Kinetic channels such as self- assembly result from processes such as solvent mixing[128], emulsification[129], or crystallization of blocks[96,130] that lead to spontaneous demixing from the natural phase separation of unlike polymer blocks to increase stability[96].

Kinetic control can be achieved through either solvent-directed manipulation or acid/ base directed complexation for block copolymers with suitable chemically compatible groups such as multifunctional organic amines and hydrophilic water compatible PAA blocks[96]. Kinetic controlled self-assembly through solvent mixing uses principles such as co-non-solvency where a mixture of solvents that are usually good solvents for a polymer are combined to produce a bad solvent for the polymer[131]. Co-non-solvency leads to a narrower particle size distribution as particle size uniformity has been found to be less achievable in good solvents due to low electrostatic stabilization since radical sites and pendant vinyl group interact between

neighboring polymer chains which grow the polymer networks sporadically leading to different size distributions[89]. If a proper balance of solvents is not achieved frustration of the forming particle can lead to saddle shapes and concentric onion morphologies[104].

Amphiphilic block copolymers are especially useful in kinetic control adding the stability of charge and forming aggregations of specific morphologies[132]. The hydrophobic regions aggregate in polar solvents and swell while in non-polar solvents while hydrophilic regions interact favorably with polar solvents, and aggregate in organic solvents. Phase separation and aggregation of unlike polymers, such as hydrophilic-hydrophobic interactions, form particles with three regions the insoluble core, a wall and a soluble corona[120]. Multiple morphologies are possible including inverted structures based on the spontaneous membrane curvature formed and the shape of lowest energy as well as vesicular types, those with a hollow internal cavity, which can hold solutes, dye, macromolecules and proteins that could be utilized in drug delivery and other applications[104,106,120]. If the copolymer used to make a microgel has more than two blocks multicompartment nanostructures[133,134,135,136] can be formed.

Here we use a guided self-assembly method carried out with ratios of good and bad solvent for a kinetically advantageous polymer aggregate. This approach has been carried out by other groups[137] where a blending of high molecular weight polymer solution in an aqueous medium produced nanoparticles of a single geometry that demixed into vesicles and multicompartment nanoparticles respectively. Experimentally for polystyrene-block-poly(acrylic acid) (PS-b-PAA) diblock copolymer the microgel morphology is influenced by the length of PS, the hydrophobic block[138]. Phase separation in solvents known as “kinetic trapping” is the phase separation of water mixed with organic solvent in solution which can produce a polymersome, an artificial polymer vesicle[139].

Physical qualities, capabilities, geometries, and methods of formation are a growing area of research. The purpose of this work is to self-assemble electrolytic microgel particles from a model triblock copolymer through the use of solvent mixing and examine the resulting structural morphology, physical properties, and particle responsiveness. Specifically, we created particles from ABA triblock copolymers, which have been found to create micelles[94] of PS-PAA-PS through self-assembly from solvent mixing. The polymer used was a triblock of (PS) and (PAA) due to their high availability, ability to be synthesized in high purity, known properties, and the electrolytic effects of PAA combined with the hydrophobic effects of PS[140]. The triblock copolymer consists of two PS end blocks with a longer chain of PAA in the middle. PS was chosen as it is well-studied hydrophobic polymer that swells in aromatic organic solvents and the PS also adds stability due to its high glass temperature[76]. PAA was chosen for its valuable properties of pH responsiveness and biocompatibility[141]. PAA is biocompatible with carboxyl groups that provide a built in responsiveness to pH[142]; PAA is also an acid which provides the opportunity for examining interactions with different solvents and salts.

Previous works have shown that PAA and PS block copolymers form structures upon dialysis with water. In the case of a diblock copolymer, as carried out by Li et al., a micelle was formed when the diblock was dissolved in water and DMF solution due to the amphiphilic chemical nature of the polymer which forms hydrogen bonds with the water[143] or in THF, water, and DMF solvent[120,144,145]. Particle size is largely dependent on the length of the PAA block of the copolymer; longer PAA blocks have higher water affinity forming more hydrogen bonds which increases the surface tension and decreases interfacial tension between the PAA segments and the PS segments, lowering free energy[98,104]. Aromatic organic solvent such as THF[89] fluidizes and swells PS while the addition of water causes the chains to aggregate and solidify[104].

This self-assembly method can be used to create microgel particles of different sizes and lengths. Use of multiple materials can be used to create different nanoscale geometries through aggregation differences creating distinct spatial morphologies[96].

Our particles are not covalently cross-linked; rather they self-assemble into a network where the solidified PS domains serve as physical crosslinks (Figure 26). The process may be guided by phase separation similar to the self-assembly of a biological vesicle[125]. At high water concentrations PAA-PS block copolymers thermodynamically favor spherical vesicle formation when dissolved in non-equilibrium co-non-solvent mixtures followed by addition of excess water. Vesicle size is the result of procedure[139]. Pochan et al. carried out a similar guided self-assembly process using water added quickly or slowly and found that it did not affect the way the polymers collapsed during aggregation. The speed affected the shape of the particles. The particles made from fast addition were only spherical while the particles formed from slow addition were spherical and cylindrical.

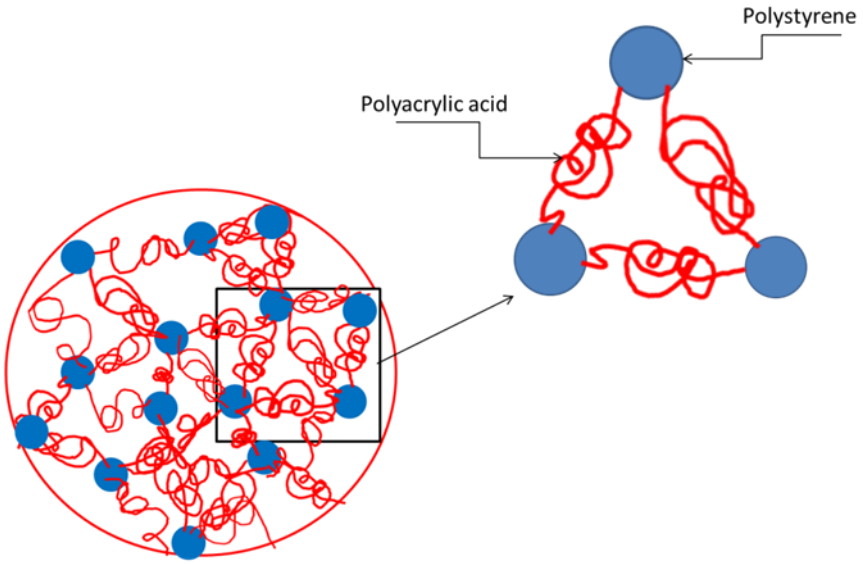

Figure 26. Representation of particle made from a triblock copolymer in which a network is formed from end group aggregation.

Theory

Classically microgel particles have been compared to hard spheres; however, the comparison is flawed. Depending on the curvature of the particle, the volume fraction, and the particle chemistry[146] the microgel particle system has been shown to have unique qualities vastly different from those of a hard sphere system. In 1D microgel particles and hard spheres behave as linear arrays of spheres subject to repulsion[104,147]; in 2D microgel particles behave more like liquids[104] while hard spheres cannot fully occupy a space and form close packing hexagonal structures. In 3D hard sphere system particles cannot occupy spaces already occupied by neighbor particles; as the number of particles increases the order increases. In general, the spheres form close packed structures which do not fully occupy a space. Microgel particles can pack to higher densities in 3D than hard spheres due to their lower repulsion forces[147] and malleable softness which results in different properties. As mentioned in the background section microgel particles exhibit non-Einstein viscosity and shear thinning[89] in colloidal suspension which allows for more dense packing than possible in hard spheres[89,116] and gives them liquid-like behavior even at high volume fractions. The decreased viscosity and ability to densely pack affects the thermodynamics of the system, for example altering crystallization temperatures and glass transitions[95]. The softer microgel particles are less fragile, or less prone to breaking, at the transition temperatures than comparable hard spheres which are more brittle. The microgels also showed stronger tendency towards suspension behavior unless protonated or affected by external stimuli compared to a similar hard sphere[91].

The underlying physics of microgel particles remains under study. Past and current theories of microgel particles mechanical properties and swelling remain insufficient to explain

diverse real world particles. Flory's theory is an approximation of how much a particle will swell in a given solvent:

$$\Phi_2 = \{\frac{X v_1}{V_c\left(\frac{1}{2} - x_{12}\right)}\}^{3}/_{5} \quad (17)$$

where X represents number of cross-links within a volume of a collapsed particle, V_c is the volume, $(\frac{x}{V_c})$ is average cross link density, and x_{12} is the Flory solvent-polymer interaction parameter. Flory's theory holds only if the assumption of uniform swelling holds, an assumption not withheld by experimentation[89]. It also falls short when dealing with non-spherical particles.

Stokes analysis, used to determine particle diameters, is based on hard spheres and does not account for other aspects of microgel particles such as hydrophobic-hydrophilic interactions, solvent interactions, or other factors affecting particle morphology[89,148]. Some groups have applied multiple theories of diameter swelling to their findings[149] to account for the shortcomings of these methods such as mixing Flory swelling with other theories such as gel elasticity[150] or polymer melts.

Particle swelling and viscosity also do not account for other aspects of particle mechanics. Most articles show the properties of their specific particles in relation to their desired applications; morphology, rheology, and diffusion rates. Most mechanical measurements and properties are also applied to large numbers of particles rather than individual particles. The story of microgel particle mechanics, therefore, remains incomplete. More individual particle mechanical measurements need to be investigated.

Experiment

Polymer Solutions

Made a solution based on previous work of our own group and other groups from literature a small amount 0.1-0.2% polymer, Poly(styrene-b-acrylic acid-b-styrene) Mn: PS(1000)-PAA(50000)-PS(1000) PDI: 1.08 or Mn: PS(1000)-PS(20000)-PS(1000) PDI: 1.23 from Polymer Source was dissolved in Tetrahydrofuran (THF) [99.9%] Fischer Scientific, if Nile red dye was added to solutions it was added to the THF. An organic diamine, N,N-Dimethylformamide (DMF) Fischer, 6 drops ~0.1g was added which complexes with PAA while PS aggregates with itself and swells in the THF. DMF is supported in literature as a good solvent for PS block copolymers. This was followed by addition of deionized water from Milli-Q at 18.2 MΩ.cm at 25 °C in a 75% ratio to the organic solvents after being allowed to sit for at least two days. A range of master solutions were created with the two triblock copolymers, different weight percentages of polymer, and amounts of Nile red dye.

Microscopy Preparations

Cut mica sheets and silicon wafers were used as substrates to observe solutions. Addition of solution onto substrate was done with glass pipette or micropipette formed from capillary tubes put through capillary tube puller. Samples were dropped onto the substrates and allowed to dry. Samples were then rehydrated with water in order to determine if particles would go back into solution and to spread them out more on the substrate for easier viewing. Prior to dye being added to solutions directly after sample drop drying step a drop of Nile red + toluene dye was added dried and followed by a drop of distilled water also allowed to dry. A few different methods of solvent based kinetic control for particle formation were used; water crashing and crashing into an organic solvent toluene to observe.

Water Crashing

Water was chosen as a good solvent for PAA and a bad solvent for PS. Distilled water was put into a glass vial (20 mL) and then triblock copolymer solution was added by a micropipette syringe apparatus, between 0.4 mL and 0.6 mL, at different ratios of water to solution including: 1:4, 1:10, 1:20, and 1:100 of master solution to water. The new solution was then removed from vial via glass pipette and drops placed on silicon wafers. The drops of solution were allowed to dry in air under observation via upright optical microscope. A drop of distilled water was then placed on the Si wafer in an effort to rehydrate and re-dissolve particles back into solution. Again observations were conducted via upright optical microscope or confocal microscope. In confocal measurements glycerol solutions, 50/50 and 99% were occasionally used in an attempt to slow down particle motion. Confocal samples were also created with mica or Si substrates covered with a coverslip to aid in imaging. Images were collected at all steps of the process. Samples were imaged with AFM following the evaporation of the second (rehydrating) water droplet.

Toluene Crashing

Toluene [99.97%] Fischer Chemical Toluene was chosen as a second solvent as it is a good solvent for PS and a bad solvent for PAA. Two procedures were used with toluene. In toluene crashing a small amount was either passed through a funnel of excess toluene and collected immediately or placed in an excess of toluene that was left on a rocking mixer overnight.

In the first method a seperatory funnel was filled with an excess of toluene. Master solution was added from the top dropwise with a glass pipette and passed through the toluene to the stopcock. The stopcock was immediately opened to extract the portion at the bottom of the

funnel, which should contain any newly formed particles. The toluene solution was then applied directly to substrate dropwise with a glass pipette; toluene drops dried before addition of subsequent drops. Vials with too much toluene were placed in a fume hood to allow the evaporation of the excess.

The second toluene crashing method involved prolonged mixing in toluene. A 20 mL vial was filled to almost the top with toluene; a small amount of copolymer solution was added (5-15 drops from a glass pipette). Additional toluene was then added to fill the vial fully; the cap of the vial was then screwed on and it was immediately placed on a wave motion lab mixer for 24 hours. After the 24 hour period the vial was removed and the sample was taken as quickly as possible from the bottom of the vial and placed dropwise onto substrate via glass pipette. Toluene was allowed to dry in between drops. Images of the resulting particles were collected with an upright optical microscope. A drop of water was added to rehydrate particles and was accompanied by more observations and imaging. At times a hot stage was used to speed the drying during the rehydration step.

Results and Discussion

PS-PAA-PS triblock was dissolved in solutions of 3:1 water to organic ratio, at other ratios the master solutions showed undissolved chunks or visible lines in solution. This finding was in keeping with literature and some previous work by Rozairo et al[151]. Some master solutions were cloudy with larger polymer concentrations, possibly indicating micelle formation. Triblock did not form particles in solution without further kinetic solvent co-non-solvency this was evident from drying master solution alone on a Si wafer as shown in Figure 27. Even after rehydration dried out master solution formed large clumps of polymer of film-like blobs which swelled with water addition and linear polymer. The large amount of polymer on the wafer

confirmed the solvents ratios in our master solutions were effective in dissolving the bulk dry polymer into solution. The large amount of polymer even led to the formation of clearly visible elastomer bubbles Figure 28.

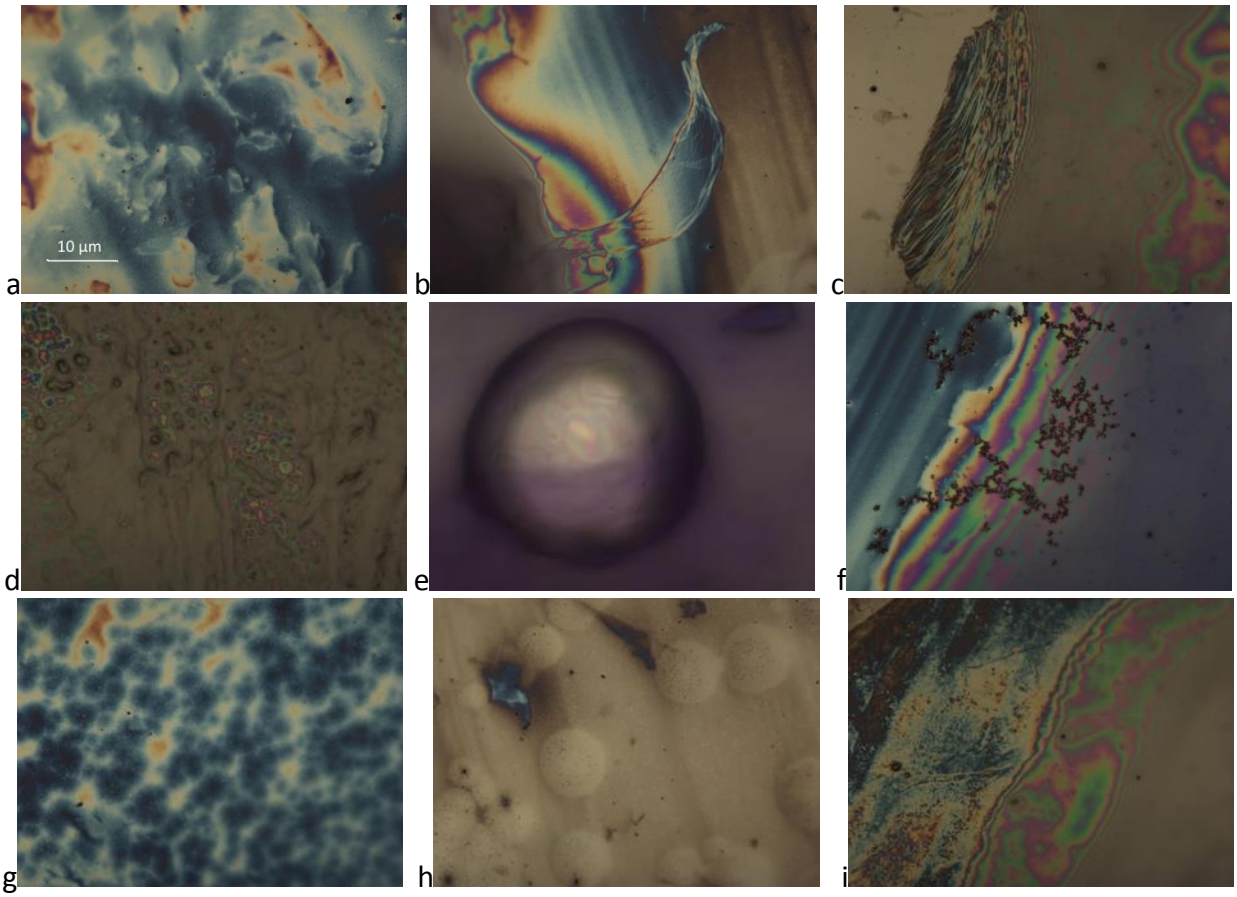

Figure 27. Master solution of PS-PAA-PS 1:50:1 ratio with added dye dried on Si wafer and rehydrated with a drop of distilled H_2O. 50x magnification. a) and b) polymer chunks from solution c) lines of polymer becoming visible as solution dries out (left is silicon, right is fluid/polymer mix) d) and e) film like blobs that swelled with rehydration f) dye crystals g), h), and i) other areas showing a sufficient amount of polymer in solution.

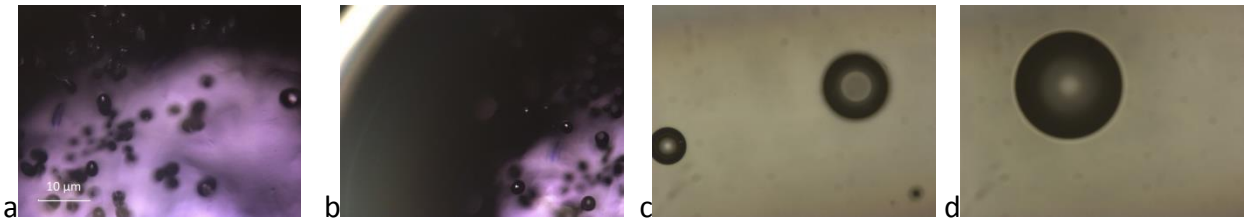

Figure 28. Elastomer bubbles ar 50x magnification on optical microscope a) and b) PS-PAA-PS 1:50:1 triblock master solution with dye in a water crashed sample, multiple elastomer bubbles formed. c) and d) elastomer bubble formation in glycerol of PS-PAA-PS 1:20:1 triblock master solution without dye.

Water Crashing

Particles were found to form at all ratios studied with the best results from higher ratios of water to master solution at 1:4 ratios and above. At lower ratios the particles did not appear to form as well with some sections still swelling under rehydration. At higher ratios, those above 1:10, excess water needed to be evaporated due to the high dilution. In Figure 29 the 1:20 water crashing ratio does not give good results due to excess water dilution which makes it less likely to locate particles. If excess water is evaporated off as in the 1:100 ratio particles are easier to locate, however, the excess water takes excess time to evaporate. Ratios between 1:4 and 1:10 were focused on as they did not have the excess water problem and produced particles consistently. The author and Alex Rice saw no discernable differences in whether water was added to master solution or master solution was added to water or in speed of water addition.

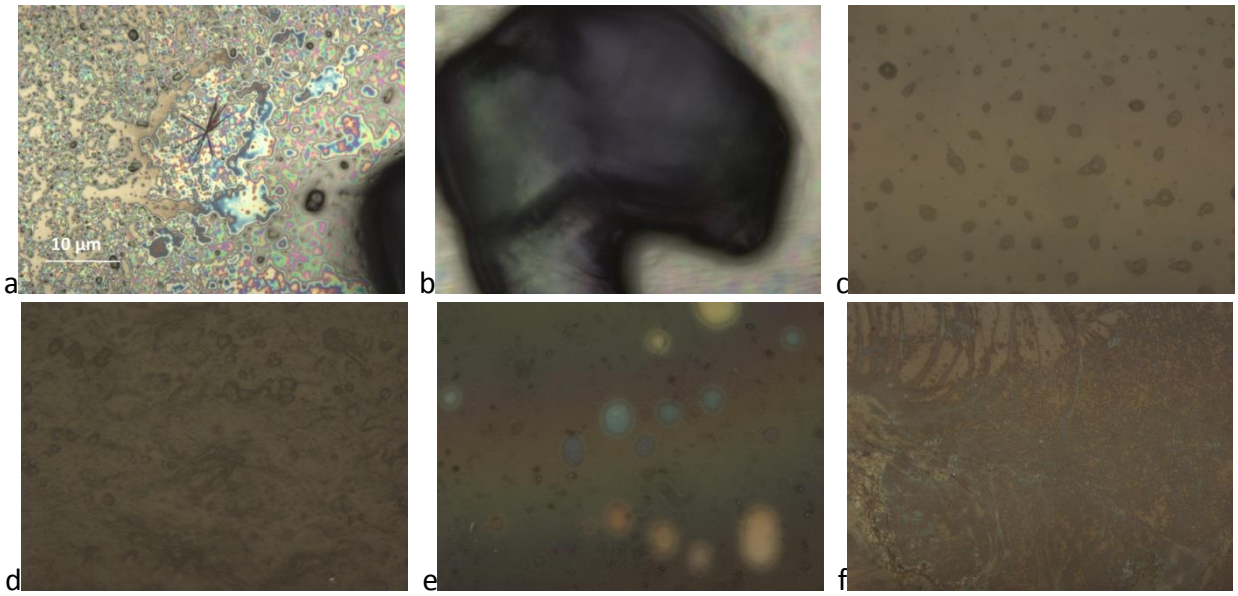

Figure 29. Different MS:water ratios of PS-PAA-PS 1:50:1 triblock at 50x magnification on optical microscope. a) and b) injected into a small amount of water below 1:4 ratio, clumps and swelling c), d) 1:10 ratio particles and blobs on mica substrate e) 1:20 ratio on mica substrate without excess water evaporation f) 1:100 ratio on mica substrate after evaporation of excess water.

During drying most samples formed concentrated central areas which were too concentrated and tall to properly image without further treatment. To spread the particles out heat drying, washers sonicated in acetone, and water hydration were found to be effective, Figure 30. The addition of a hot stage to the sample drying process resulted in more spread out particles. The particles were spatially separated; however, the morphology of the resultant particles seemed different than samples allowed to dry in ambient temperatures. Placing the sample in the center of a washer in order to draw out the corners of the solution as it dried was somewhat effective, however, some solution would go underneath of the washer resulting in less particles on the undisturbed substrate. Water rehydration alone did not spread out the particles sufficiently unless pipette was used to physically move them or small amount was moved to another location.

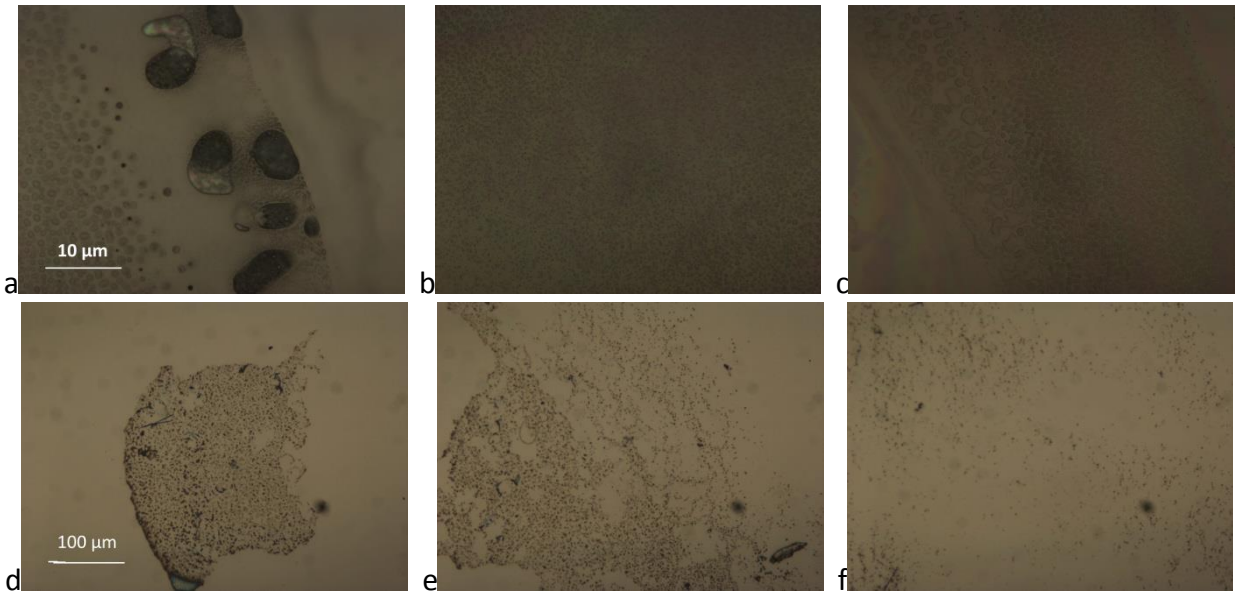

Figure 30. PS-PAA-PS 1:50:1 triblock a), b), c) 1:10 ratio water crashing and heat assisted solvent evaporation at 50x magnification. d) sample dried in center of washer at 5x magnification e) and f) at 50x magnification.

Samples showed some difference in overall morphology between the different length triblock copolymers and the different master solutions. Figure 31 shows the morphology of

different solutions at 1:4 ratios. AFM was used to image morphology and texture to determine if the polymer formed discrete particles, film-like blobs, or disorganized polymer clumps. The AFM provided shapes of formations and size ranges. Tapping mode was used in order to distinguish between the soft PAA blocks and the harder solidified PS aggregate blocks. Longer triblock copolymer, that at 1:50:1 ratio, showed consistent morphology as shown in Figure 32 where the particles appear as round flattened pancakes which is in keeping with literature observations[89] of microgel spheres upon solvent evaporation. The dye also did not appear to have any effect on morphology. The shorter polymer showed a more diverse irregular morphology between solutions although all appeared to make particles.

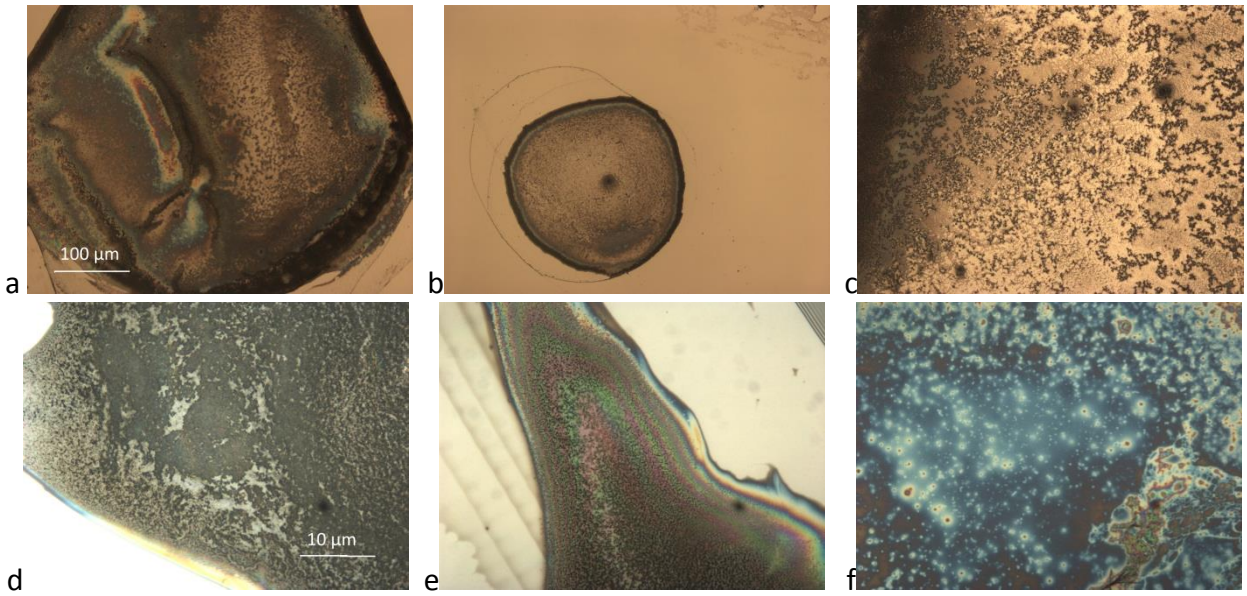

Figure 31. PS-PAA-PS 1:50:1 with dye at 1:4 ratio MS: water dried and rehydrated a), b), c) are at 5x magnification d), e), and f) are at 50x magnification.

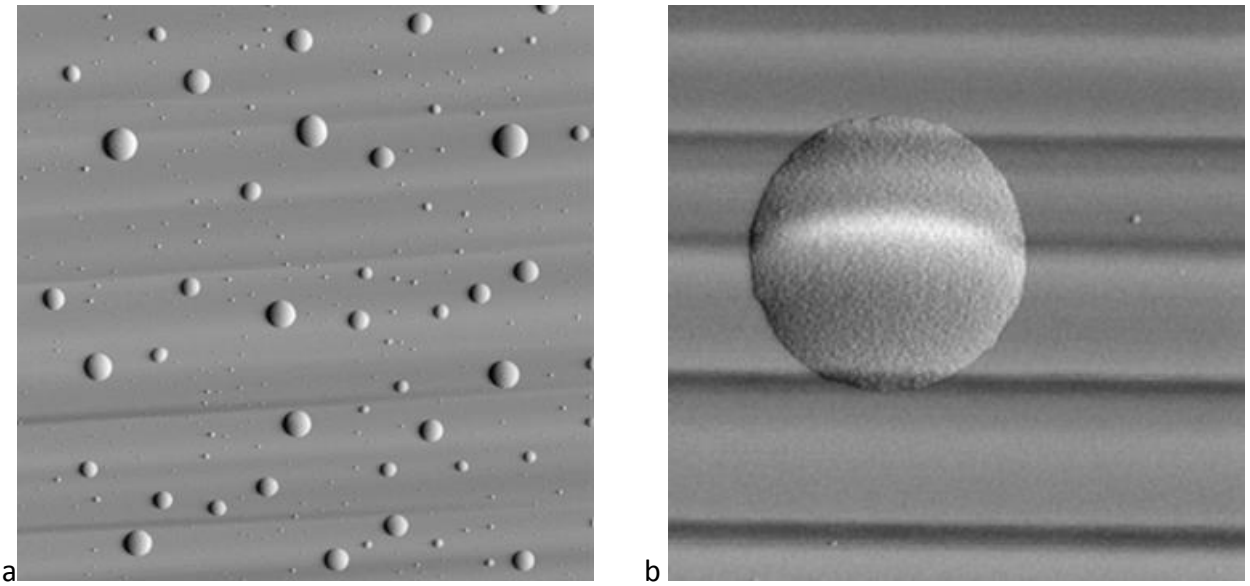

Figure 32. AFM imaging of 1:4 water crashed PS(1000)-PAA(50000)-PS(1000) master solution with dye a) 20000 nm x 20000 nm image with height range ~35-80 nm b) 2000 nm x 2000 nm with 67.6 nm height.

The shorter triblock copolymer, 1:20:1 ratio, showed particles with a variety of morphologies upon drying on a substrate as seen in Figure 33. We identified a lacy pattern morphology, a concentrated particle morphology, and areas of spread out individual circular particles. At 5x magnification the varying topography is clearly discernable. Imaged with AFM, Figure 34, the edges appear taller and steeper with less regularity of shape. The forms appear to be discrete particles just as with the longer polymer particles. Polymers of the same composition even of different lengths both form particles. The particles appeared spherical and circular at 1:4 ratio, MS: water, imaged with SEM and as clumps at 1:9 ratio, Figure 35 (samples prepared by Alex Rice). There were some impurities that crystallized inside of the particles but it did not prevent particle formation.

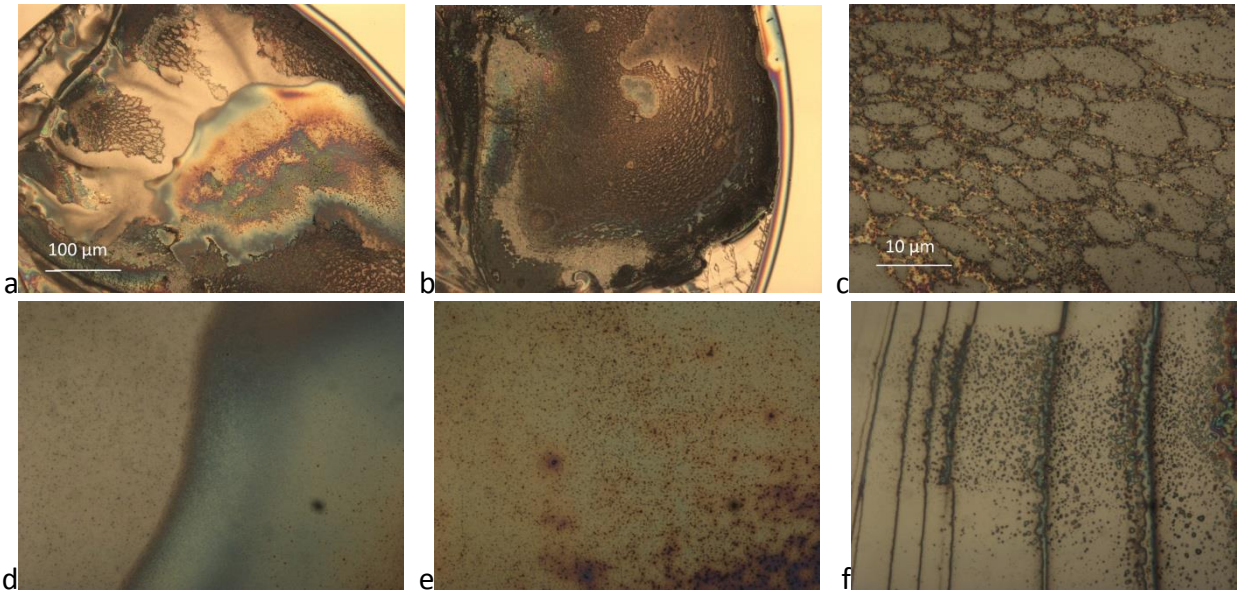

Figure 33. PS-PAA-PS 1:20:1 ratio at 1:4 water crashing after rehydration a) and b) are at 5x magnification c), d), e), f) are at 50x magnification from different areas of a) and b) and surroundings on the substrate.

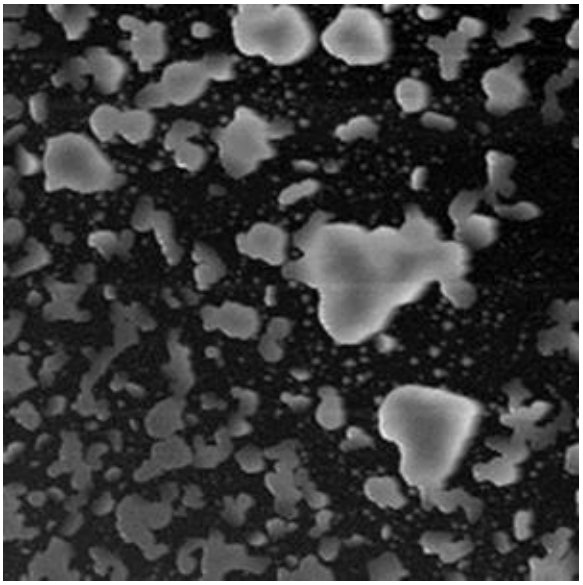

Figure 34. AMF micrograph of 1:20:1 PS-PAA-PS water crashed at 1:4 ratio. Imaged area was 10000 nm x 10000 nm with a height range of ~90-230 nm.

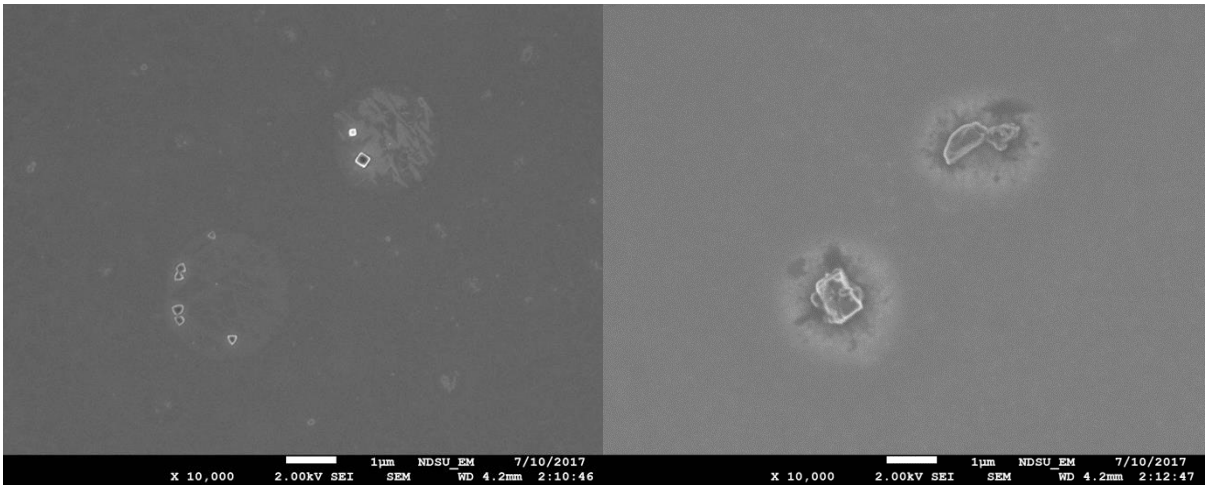

Figure 35. SEM images of water crashed PS-PAA-PS 1:20:1. 1:4 MS: water (left) 1:9 MS: water (right).

Over multiple tests results were consistent as can be seen in Figure 36 and Figure 37 which shows samples of 1:4 water crashing carried out on 4 separate days of 1:20:1 triblock copolymer. Although there are some differences the overall appearance of particles is similar. This supports that particle formation is consistent and repeatable. The approach of co-non-solvent crashing into water shows good microgel particle formation for all variables that we tested.

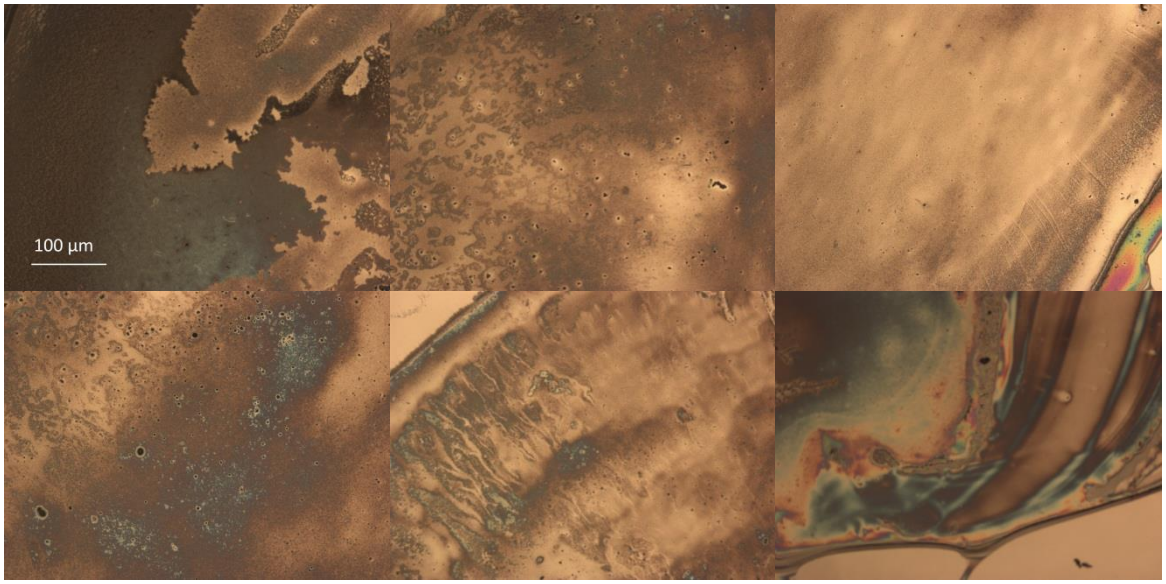

Figure 36. PS-PAA-PS 1:20:1 in a 1:4 water crashing at 5x magnification, the first 5 from one day and the last from a different day.

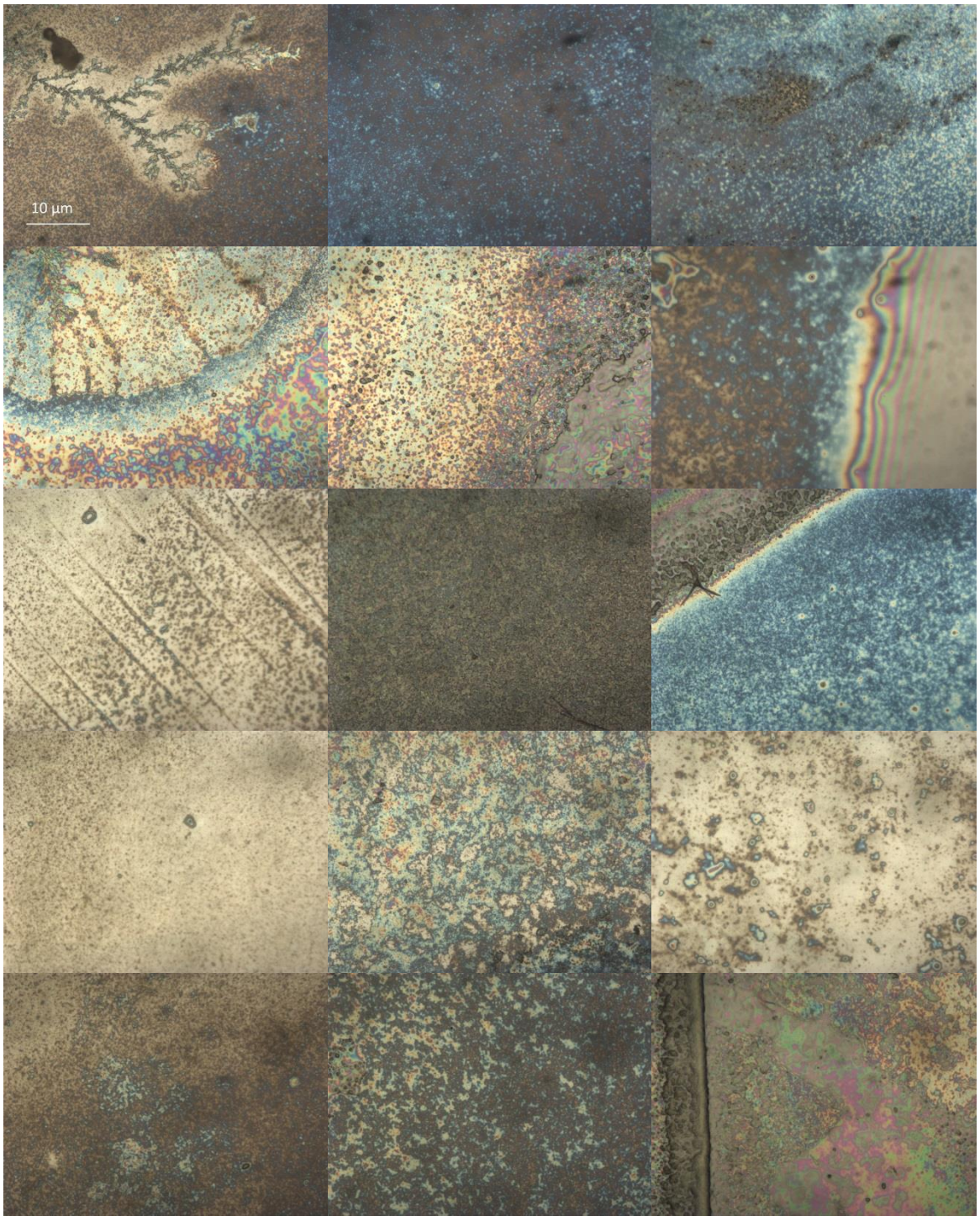

Figure 37. PS-PAA-PS 1:20:1 in 1:4 water crashing taken on 4 different days from 4 different samples at 50x magnification.

Particles were not visible in solution by optical microscopy. With dye they were somewhat visible by laser scanning confocal microscopy (Figure 38 and Figure 39). It was

challenging to discern what might have been particles and what might have been noise. There was also a large amount of polymer that remained stuck to the Si wafer which leads to doubt that an appreciable amount of polymer dissolved back into the water as particles. This sticking and almost film formation is attributable to possible attraction between the particles and the substrate or between the particles and themselves that keeps them from separating and dissolving into solution.

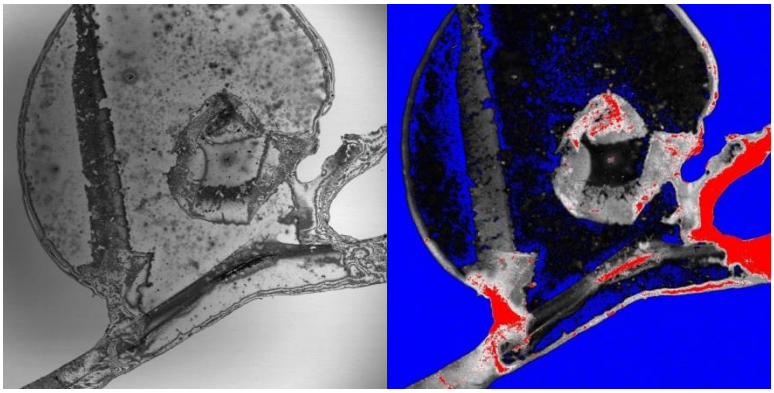

Figure 38. Confocal imaging of PS-PAA-PS 1:50:1 crashed water in 1:4 ratio rehydrated at 10x magnification. The left image is the channel showing the sample under visible light spectrum. The right image is from the channel that imaged the sample under blue fluorescent laser.

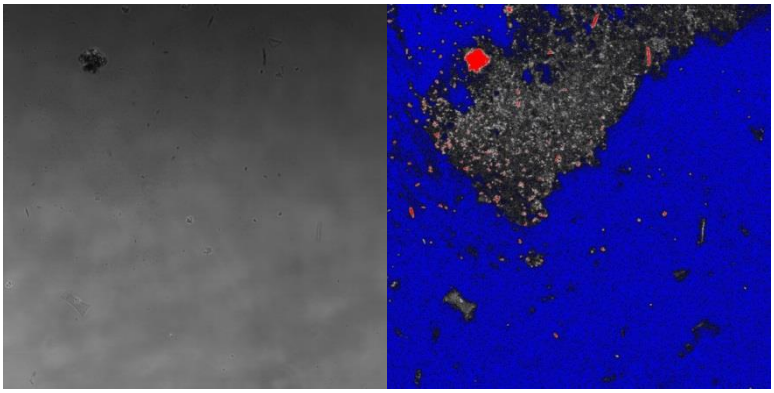

Figure 39. Confocal imaging at 50x of PS-PAA-PS 1:50:1 ratio crashing in water 1:4 and rehydrated, viewed at 50x with dyed particles visible under fluorescence channel on the right.

In order to better observe the particles if they do return to solution index mismatched microscopy was carried out on an undyed sample. DIC index mismatching microscopy as in

Figure 40 showed small clear spheres in solution and on a piece of glass debris on the bottom. These spheres were also evident at other areas higher in the solution.

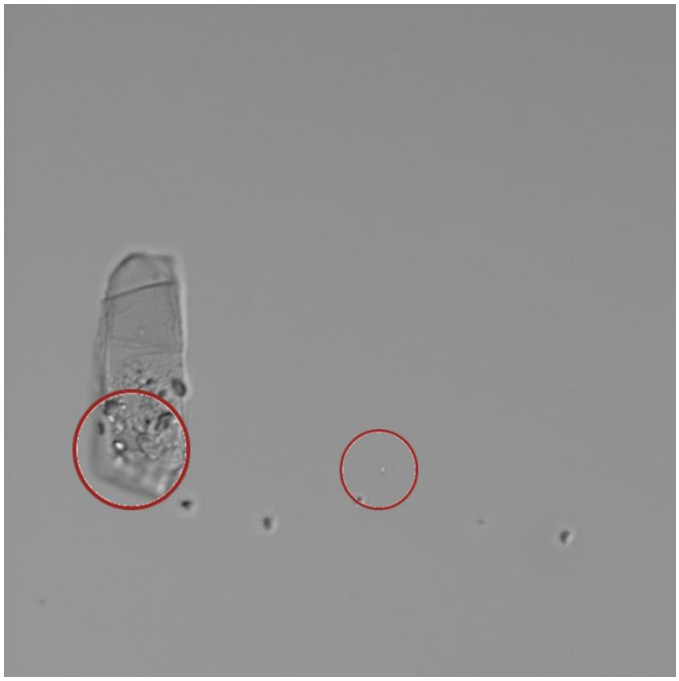

Figure 40. Particles visible in solution and on glass from PS-PAA-PS 1:20:1 ratio in water viewed on Zeiss microscope LSM-T-PMT Define focus with HAL 100 attachment Zen 2011 software.

Toluene Crashing

Crashing in toluene gave different morphologies than that of water crashing. The particles were generally more discrete and separate, lizard skin or shark skin patterns were seen, and some particles were macroscopic. Morphology was the result of the specific method used: toluene crashing in vial, toluene crashing in vial with mixing, and toluene crashing through excess in seperatory funnel. All samples were rehydrated just as in water crashing.

Toluene crashing involving master solution added dropwise into a vial full of toluene produced sparse particles Figure 41 and those with a topology that resembles irregular squiggle patterns Figure 42. The water ends up at the bottom of the vial as it separates from the toluene. When the toluene was mixed in the vial the resulting morphology was that of a lizard skin Figure

43, enhanced by heating Figure 44, or that of egg shaped particles depending on the polymer length 1:50:1 resulted in lizard skin morphology while 1:20:1 resulted in egg shapes.

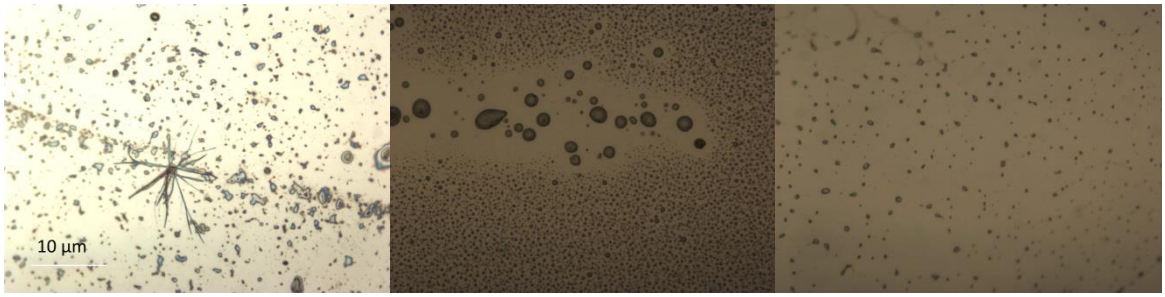

Figure 41. PS-PAA-PS 1:50:1 added dropwise to ~20mL of toluene at 50x magnification.

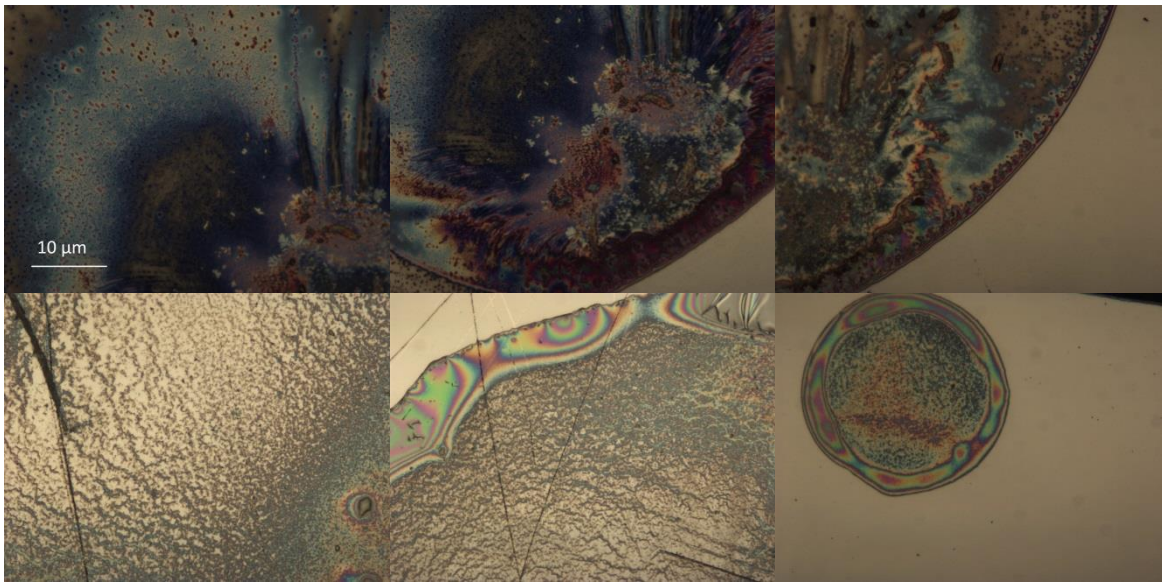

Figure 42. PS-PAA-PS 1:50:1 added dropwise to ~20mL of toluene at 50x magnification concentrated a) dried with heater b) through f) were dried in air.

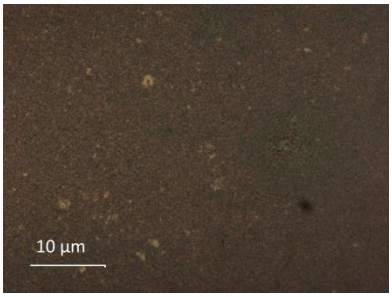

Figure 43. PS-PAA-PA 1:50:1 mixed in excess toluene for 24 hours allowed to dry in air and rehydrated.

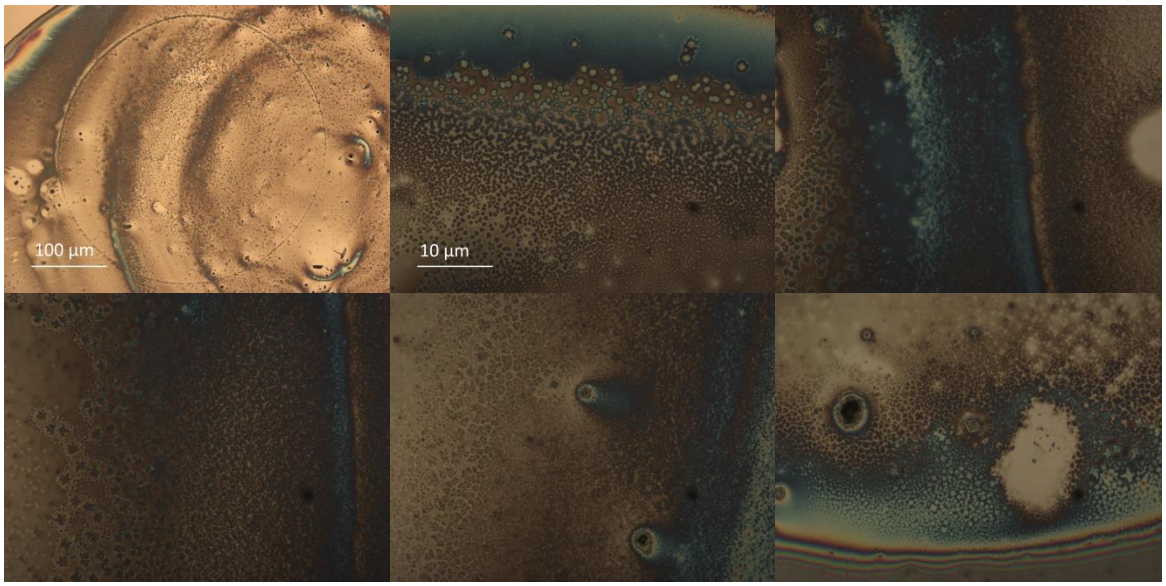

Figure 44. PS-PAA-PA 1:50:1 mixed in excess toluene for 24 hours rehydrated and dried at 70 °C on a hot plate a) 5x magnification b) through i) 50x magnification.

AFM images were taken of the lizard skin sample in order to determine the particle morphology. As shown in Figure 45 the sides are highly folded in like flowers or broccoli. This is probably due to interaction between PAA and toluene which leads to the microgel forming differently than the spherical mesh that we hypothesized and observed in water crashing. The PS blocks would not aggregate in toluene until the particle entered the small amount of water in the bottom of the vial.

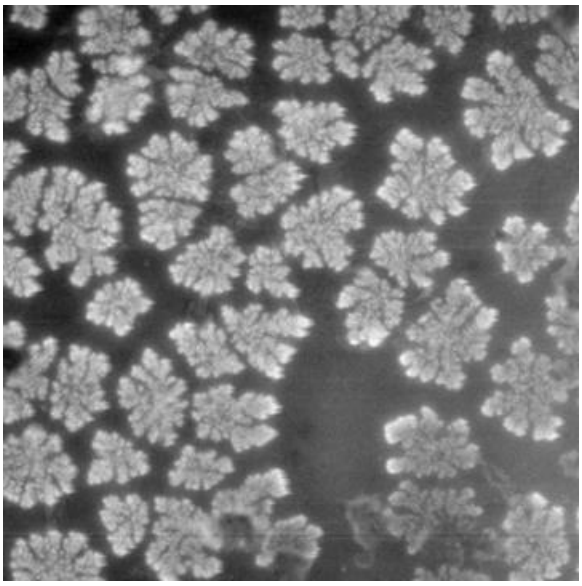

Figure 45. PS-PAA-PS 1:50:1 mixed in toluene and heat dried. AFM image scan size 10000 nm x 10000 nm of height range ~20-50 nm.

The egg shaped particles were formed in toluene crashing for the shorter polymer 1:20:1. The particles are so large that they are visible at low magnification as can be seen in Figure 46. At higher magnifications all three of the above mentioned types are present, distinct particles, lizard skins/ blue marble patterns, and egg like particles with center and surrounding haloes, Figure 47. This method bares further investigation for particle morphology.

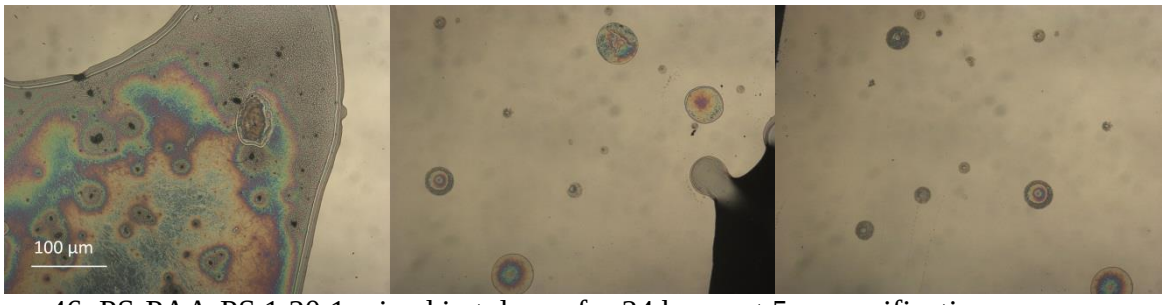

Figure 46: PS-PAA-PS 1:20:1 mixed in toluene for 24 hours at 5x magnification.

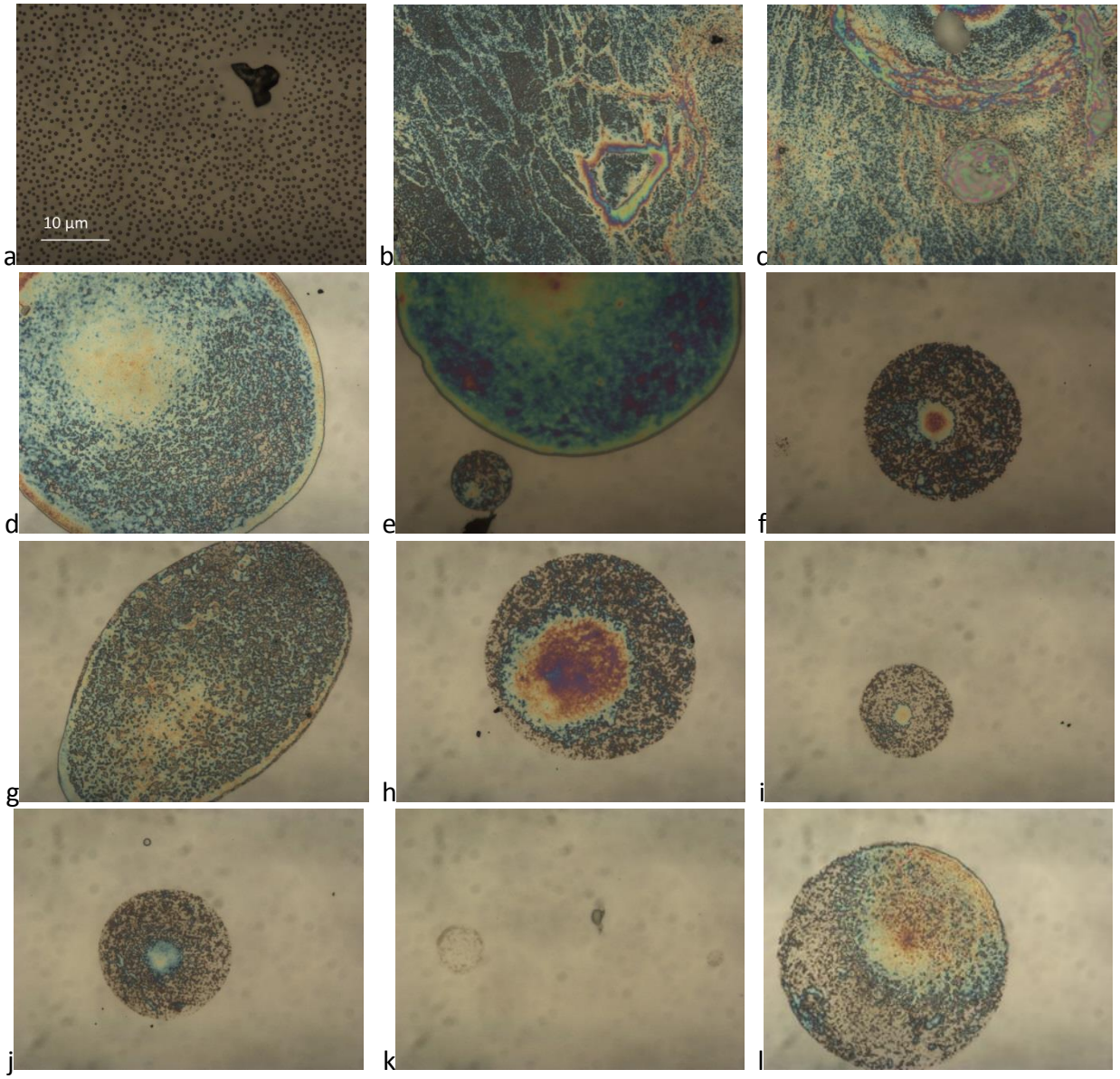

Figure 47. PS-PAA-PS 1:20:1 mixed in toluene for 24 hours 3 different patterns a) discrete particles, b) and c) lizard skin d) through l) haloed particles.

Seperatory funnel results were less conclusive to the formation of particles. The same problem as in high ratios of water crashing was evident depending on how quickly the stop cock was closed as large amounts of excess toluene also took some time to evaporate. Taking from the bottom (the water layer) resulted in a thin layer of particles, Figure 48. In the presence of dye large crystalline chunks resulted from drying, Figure 49. This method was most similar to dropping MS into a vial of toluene. The difference in shape seems to be the result of agitation.

This method also bares further investigation of the morphology of the spread out particles that are produced.

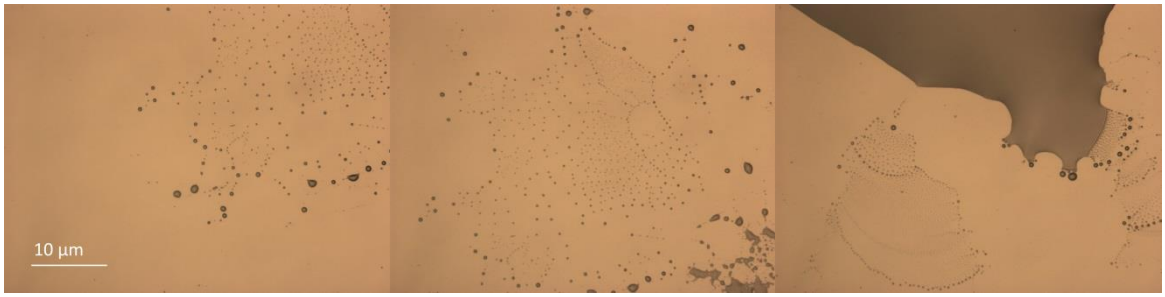

Figure 48. PS-PAA-PS 1:20:1 passed through excess toluene in seperatory funnel at 50x magnification.

Figure 49. PS-PAA-PS 1:50:1 passed through excess toluene in seperatory funnel at 50x magnification.

Conclusion

All three methods of kinetic self-assembly appeared to form particles of different morphologies. For water the ratio of MS to water and the speed of addition did not appear to affect particle morphology formed. The longer polymer appeared to form rounder particles than the shorter polymer, possibly due to the decrease in the PAA chain length. In toluene crashing three distinct patterns were produced: discrete particles, lizard skin, and egg like particles. The lizard skin was highly indented when viewed with AFM but still displayed distinct same size particles. The main difference in particle formation in toluene systems appeared to be the presence or absence of agitation during the MS into solvent mixing stage.

REFERENCES

[1] R. A. L. Jones, Soft Condensed Matter (Oxford university press, Oxford, New Yoke, 2002), 16.

[2] H. R. Allcock, Introduction to Materials Chemistry (John Wiley & Sons, Inc. Hoboken, New Jersey, 2008), 118.

[3] G. Odian, Principles of Polymerization (John Wiley & Sons, Inc., Hoboken, New Jersey, 2004), Fourth edition, 32.

[4] A. Voronov, course CPM 673 class lectures, NDSU, Fall 2016.

[5] P. G. De Gennes, Journal of Polymer Science Part B: Polymer Physics, 43, 2005.

[6] P. G. de Gennes, European Physics Journal E, 23, 3, 2007.

[7] P. G. De Gennes, Faraday Discussions of the Chemical Society, 91, 96, 1991.

[8] P. G. De Gennes, Journal Physique, 31, 235, 1970.

[9] G. R. Strobl, The Physics of Polymers Concepts for Understanding Their Structures and Behavior (Springer-Berlag, Heidelberg, Berlin, 2007) Second Corrected Edition, 1.

[10] P. G. De Gennes, The Journal of Chemical Physics, 66, 5825, 1977.

[11] P. Cordier, F. Tournilhac, C. Soulié-Ziakovic, L. Leibler, Nature, 451:7181), 977, 2008.

[12] J. Diani, B. Fayolle, P. Gilormini, European Polymer Journal, 45, 601, 2009.

[13] D. R. Xin, Q. Han, Journal of Molecular Modeling, 21, 5, 2015.

[14] RTM resins – a users' guide Special Feature Reinforced Plastics, 22, 1992.

[15] Y. Choi course, MNT class lectures, 2016.

[16] P. G. De Gennes, European Physics Journal E, 2, 201–205, 2000.

[17] J. L. Keddie, R. A. L. Jones, R. A. Cory, Faraday Discussions, 98, 219, 1994.

[18] J. Ferry, Viscoelastic Properties of Polymers (Wiley, New York, 1970).

[19] O. A. Saleh, The Journal of Chemical Physics, 142, 194902, 2015.

[20] T. Annable, R. Buscall, R. Ettelaie, D. Whittlestone, Journal of Rheology, 37, 695, 1993.

[21] H. G. Allen, Analysis and Design of Structured Sandwich Panels, (Pergamon Press, New York, NY, 1969) 178.

[22] Y. Ebata, A. B. Croll, A. J. Crosby, Soft Matter, 8, 9086, 2012.

[23] E. J. Kramer, Journal Advanced Polymer Science, 53, 1, 1983.

[24] C. Maestrini, E. J. Kramer, Polymer, 32:4, 1991.

[25] R. Tang, H. Huang, H. Tu, H. Liang, M. Liang, Z. Song, Y. Xu, H. Jiang, H. Yu, Applied Physics Letters 104, 083501, 2014.

[26] Y. Zhang, Y. Huang , J. A. Rogers, Current Opinion in Solid State and Materials Science, 19, 190, 2015.

[27] M. Hasanzadeh , N. Shadjou, Materials Science and Engineering C, 61, 979, 2016.

[28] J. H. Cho, M. D. Keung, N. Verellen, L. Lagae, V. V. Moshchalkov, P. VanDorpe, D. H. Gracias, Small, 7, 1943, 2011.

[29] H. Liu, H. Qing, Z. Lia, Y. L. Hana, M. Lina, H. Yang, A. Lie, T. J. Lub, F. Lib, F. Xu . Materials Science and Engineering Review, 112, 1, 2017.

[30] R. A. Karnik, A. Löchtefeld, M. Subramanian, S. Bødker , S. Brewster , Morphees: toward high “shape resolution” in self-actuated flexible mobile devices, Proc SIGCHI Conference on Human Factors in Computing (Syst. Paris, France: ACM Press, 2013), 593.

[31] E. Mark, Automation in Construction, 22, 2, 2012.

[32] C. Liu, Y. Shi, Aerospace Science Technology, 53, 267, 2016.

[33] Q. Tao, C. Wang, Z. Xue, Z. Xie, H. Tan, Acta Astronaut, 128, 551, 2016.

[34] Y. Liu, J. Genzer, M. D. Dickey, Progress in Polymer Science, 52, 79, 2016.

[35] W. M. Huang, H. B. Lu, Y. Zhao , Z. Ding , C. C. Wang, J. L. Zhang , L. Sun , J. Fu, X. Y. Gao, Materials and Design, 59, 176, 2014.

[36] L. Lia, W. Lia, H. Yanga, C. Maa, J. Yua, M. Yana, X. Song, Electrochimica Acta, 120, 102, 2014.

[37] D. Akinwande, C. J. Brennan, J. S. Bunch, P. Egberts, J. R. Felts, H. Gao, R. Huang, J. S. Kim, T. Li, Y. Li, K. M. Liecht, N. Lu, H. S. Park, E. J. Reed, P. Wang, B. I. Yakobson, T. Zhang, Y. W. Zhang, Y. Zhou, Y. Zhu, Extreme Mechanics Letters, 13, 42, 2017.

[38] J. R. Allensworth, Y. Liu, H. Braun, J. Genzer, M. D. Dickey, Polymer, 55:23, 5847, 2014.

[39] C. Lauff, T. W. Simpson, M. Frecker , Z. Ounaies, S. Ahmed, P. von Lockette, R. Strzelec, R. Sheridan, J. M. Lien, ASME, 1, 2014.

[40] E. A. Peraza-Hernandez, D. J. Hartl, R. J. Malak Jr, D. C. Lagoudas, Smart Materials and Structures, 23, 94001, 2014.

[41] S. Rohmer, et al. Geometric and topological modelling of 3d crumpled structures in: DS 75-4: Proceedings of the 19th International Conference on Engineering Design (ICED13), Design for Harmonies, 4: Product, Service and Systems Design, (Seoul Seoul, Korea, 2013), 4.

[42] J. L. Miller, Physics Today, 64:10, 15, 2011.

[43] L. Bevilacqua, Applied Mathematical Modelling, 28:6, 547, 2004.

[44] T. A. Witten, Reviews of Modern Physics, 79, 643, 2007.

[45] T. A. Witten, S. R. Nagel, Physical Review Letters, 88, 076101, 2002.

[46] J. Na, A. Evans, J. Bae, M. Chiappelli, C. Santangelo, R. Lang, T. Hull, R. Hayward, Advanced Materials, 27, 79, 2015.

[47] Z. Wei, Z. Guo, L. Dudte, H. Liang, L. Mahadevan, Physical Review Letters, 110, 215501, 2013.

[48] T. G. Leong, A. M. Zarafshar, D. H. Gracias, Small, 6, 792, 2010.

[49] E. A. Peraza Hernandez, S. Hu, H. W. Kung, D. Hartl, E. Akleman, Computers & Graphics, 37, 730, 2013.

[50] L. Mahadevan, S. Rica, Science, 307, 5716, 1740, 2005.

[51] F. Lechenault, B. Thiria, M. Abba-Bedia, Physical Review Letters, 112, 244301, 2014.

[52] W. J. Arora , H. I. Smith , G. Barbastathis, Microelectronic Engineering, 84, 1454, 2007.

[53] J. Caia,, Z. Ren, Y. Ding, X. Deng, Y. Xu, J. Fenge, Aerospace Science and Technology, 67, 343, 2017.

[54] A. Chiche, C. M. Stafford, J. T. Cabral, Soft Matter, 4, 2360, 2008.

[55] K. Efimenko, M. Rackaitis, E. Manias, A. Vaziri, L. Mahadevan, J. Genzer, Nature Materials, 4, 293, 2005.

[56] F. Schneider, T. Fellner, J. Wilde, U. Wallrabe, Journal of Micromechanics and Microengineering, 18, 065008, 2008.

[57] J. Mark, Polymer Data Handbook (Oxford Univ. Press, New York, 1999).

[58] I. D. Johnston, D. K. McCluskey, C. K. L. Tan, M. C. Tracey, Journal of Micromechanics and Microengineering, 24, 035017, 2014.

[59] Dialectric Corporation, Retrieved December 12, 2017, http://www.dielectriccorp.com/downloads/thermoplastics/lexan.pdf.

[60] Bekele J. Gurmessa and Andrew B. Croll, Physical Review Letters, 110, 07430 (2013).

[61] Boedeker Plastics, Inc., Shiner, Texas, USA, Retrieved December 12, 2017, www.boedeker.com.

[62] The Engineering Toolbox, Retrieved December 12, 2017, https://www.engineeringtoolbox.com/polymer-properties-d_1222.html.

[63] Matbase, Retrieved December 12, 2017, https://www.matbase.com/.

[64] X. Li, H. A. Hristov, A. F. Yee, Polymer, 36:4, 759, 1995.

[65] Gallina USA, Retrieved December 12, 2017, http://gallinausa.com/.

[66] C. Singer, E. J. Holmgard, A. R. Hall (eds), A History of Technology, (Oxford University Press, New York, 1954).

[67] A. M. Abd, El-Khalek, Materials Science and Engineering: A, 500:1–2, 176, 2009.

[68] R. A. L. Jones, Soft Condensed Matter (Oxford university press, Oxford, New Yoke, 2002), 16.

[69] J. E. Pye, K. A. Rohald, E. A. Baker, C. B. Roth, Macromolecules, 43, 8296, 2010.

[70] K. Paeng, S. F. Swallen, M. D. Ediger, Journal of the American Chemical Society, 133:22, 8444, 2011.

[71] W. M. Lai, D. Rubin, E. Krempl, Introduction to Continuum Mechanics (Pergamon Press Inc., Elmsford, New York, 1974) 239.

[72] L.D. Landau, E. M. Lifshitz. Course of Theoretical Physics Volume 7 Theory of Elasticity (Pergamon Press, Elmsford, New York, 1986) Third Edition, 1.

[73] J. J. O'Dwyer, College Physics (Wadsworth Publishing Company, Belmont, California, 1981), 183.

[74] R. Lakes, Science, 235, 1987.

[75] A. Siber, H. Buljan, Physical Review E., 83, 067601, 2011.

[76] Croll group, private communications.

[77] W. G. Knauss, I. Emri, H. Lu, Mechanics of Polymers, 2006

[78] M. VanLandingham, P. Drzal, C. White. MRS Proceedings, 841, 2004.

[79] M. VanLandingham, N. K. Chang, P. L. Drzal, C. C. White, S. H. Chang, Polymer Science, 43:14, 1794, 2005.

[80] N. N. Peschanskaya, P. N. Yakushev, V. M. Egorov, V. A. Bershtein, L. Bokobza, Physics of the Solid State, 44:9, 1684, 2002.

[81] M. D. Shelby, G. L. Wilkes, Polymer, 39:26, 6767, 1998.

[82] P. A. O'Connell, S. A. Hutcheson, G. B. McKenna, Polymer Science, 46:18, 1952, 2008.

[83] H. Bodiguel, C. Fretigny, Macromolecules, 40:20, 7291, 2007.

[84] E. Cerda, S. Chaieb, F. Melo, L. Mahadevan, Nature, 401, 1999.

[85] S. Komura, K. Tamura, T. Kato, European Physical Journal E, 18, 343, 2005.

[86] T. Mora, A. Boudaoud, Europhysics Letters, 5:1, 41, 2002.

[87] A. E. H. Love, A Treatise on the Mathematical Theory of Elasticity (Dover, New York, 1944).

[88] T. Liang, T. A. Witten, Physical Review E 71, 016612, 2005.

[89] B. R. Saunders, B. Vincent, Advances in Colloid and Interface Science, 80, 1, 1999.

[90] G. E. Morris, B. Vincent, M. J. Snowden, Journal of Colloid Interface Science, 190, 198, 1997.

[91] A. Lyon, A. Fernandez-Nieves, Annual Review Physical Chemistry, 63,25, 2012.

[92] D. E. Discher, A. Eisenberg, Science, 2979, 967, 2002.

[93] R. H. Pelton , Adv. Colloid Interface Science, 85, 1, 2000.

[94] C. de las Heras Alarco´n, S. Pennadam, C. Alexander, Chemical Society Review, 34, 276, 2005.

[95] J. Mattsson, H. M. Wyss, A. Fernandez-Nieves, K. Miyazaki, Z. Hu, Nature, 462, 83, 2009.

[96] D. J. Pochan, J. Zhu, K. Zhang, K. L. Wooley, C. Miesch, T. Emrick, Soft Matter, 7, 2500, 2011.

[97] W. O. Baker, Industrial & Engineering Chemistry, 41, 511, 1949.

[98] R. A. L. Jones, Soft Condensed Matter (Oxford university press, Oxford, New Yoke, 2002), 16.

[99] T. Tanaka, D. J. Fillmore, Journal Chemical Physics, 70, 1214, 1979.

[100] C. Pichot, Current Opinion in Colloid & Interface Science, 9, 213, 2004.

[101] R. Messing, A. M. Schmidt, Polymer Chemistry, 2, 18, 2011.

[102] G. R. Hendrickson, L. A. Lyon, Angewandte Chemie International Edition in England, 49, 2193, 2010.

[103] P. Bouillot, B. Vincent, Colloid Polymer Science, 278, 74, 2000.

[104] K. Kita-Tokarczyk, J. Grumelard, T. Haefele, W. MeierBlock, Polymer, 46, 3540, 2005.

[105] L. A. Lyon, J. D. Debord, S. B. Debord, C. D. Jones, J. G. McGrath, M. J. Serpe, Journal Physical Chemistry B, 108, 19099, 2004.

[106] K. S. Soni, S. S. Desale, T. K. Bronich, Journal of Controlled Release, 240, 109, 2016.

[107] Z. B. Hu, X. H. Lu, J. Gao, Advanced Materials, 13, 1708, 2001.

[108] J. D. Debord, L. A. Lyon, Journal Physical Chemistry B, 104, 6327, 2000.

[109] P. Pieranski, Contemporary Physics, 24, 25, 1983.

[110] M. Huiru, G. Jianguo, Y. Runzhang, Joumal of Wuhan University of Technology - Material Science Education, 40:4, 43, 2005.

[111] H. M. Princen, Journal Colloid Interface Science, 91, 160, 1983.

[112] T. G. Mason, J. Bibette, D. A. Weitz D.A., Physical Review Letters, 1995.

[113] M. Cloitre, R. Borrega, L. Leibler, Physical Review Letters, 85, 4819, 2051, 2002.

[114] M. Cloitre, R. Borrega, F. Monti, L. Leibler, Physical Review Letters, 90, 068303, 2003.

[115] A. Einstein, Annals of Physics (Leipz.) 19, 371, 1906.

[116] M. E. Mackay, T. T. Dao, A. Tuteja, D. L. Ho, B. Van Horn, H. Kim, C. J. Hawker, Nature Materials, 2, 2003.

[117] C. D. Jones, L. A. Lyon, Journal of American Chemical Society, 125, 460, 2003.

[118] C. D. Jones, M. J. Serpe, L. Schroeder, L. A. Lyon, Journal of American Chemical Society, 125, 5292, 2003.

[119] A. N. St. John, L. A. Lyon, Journal Physical Chemistry B, 112, 11258, 2008.

[120] R. Vyhnalkova, A. H. E. Muller, A. Eisenberg, Langmuir, 30, 5031, 2014.

[121] R. H. Pelton, P. Chibante, Colloids and Surfaces, 120, 247, 1986.

[122] J. Clarke, B. J. Vincent, Journal of the Chemical Society, Faraday Transactions 1, 77, 1831, 1981.

[123] M. Antionietti, T. Pakula, W. Bremser, Macromolecules, 28, 4227, 1995.

[124] B. Neyret, B. Vincent, Polymer, 38, 6129, 1997.

[125] M. Frank, W. Burchard, Makromol. Chemical Rapid Communications, 12, 645, 1991.

[126] T. K. Bronich, P. A. Keifer, L. S. Shlyakhtenko, A. V. Kabanov, Journal of American Chemical Society, 127, 8236, 2005.

[127] R. K. O'Reilly, C. J. Hawker, K. L. Wooley, Chemical Society Reviews, 35, 1068, 2006.

[128] C. Liu, M. A. Hillmyer, T. P. Lodge, Langmuir, 24, 12001, 2008.

[129] R. Zheng, G. Liu, X. Yan, Journal of American Chemical Society, 127, 15358, 2005.

[130] Z. H. Lu, G. J. Liu, F. T. Liu, Macromolecules, 34, 8814, 2001.

[131] X. S. Wang, G. Guerin, H. Wang, Y. Wang, I. Manners, M. A. Winnik, Science, 317, 644, 2007.

[132] W. McPhee, K. C. Tam, R. Pelton, Journal of Colloid and Interface Science, 4, 156, 1993.

[133] J. H. Holtz, S. A. Asher, Nature, 389, 829, 1997.

[134] Z. B. Li, E. Kesselman, Y. Talmon, M. A. Hillmyer, T. P. Lodge, Science, 306, 98, 2004.

[135] Z. B. Li, M. A. Hillmyer, T. P. Lodge, Nano Letters, 6, 1245, 2006.

[136] F. Schacher, A. Walther, A. H. E. Muller, Langmuir, 25, 10962, 2009.

[137] B. Fang, A. Walther, A. Wolf, Y. Xu, J. Yuan, A. H. E. Muller, Angewandte Chemie International Edition, 48, 2877, 2009.

[138] H. Xu, F. Meng, Z. Zhong, Journal of Materials Chemistry, 19, 4183, 2009.

[139] L. Zhang, A. Eisenberg, Science, 268, 1728, 1995.

[140] P. Lim Soo, A. Eisenberg, Journal Polymer Science, Part B: Polymer Physics, 42, 923, 2004.

[141] G. H. Li, C. G. Cho, Korean Journal of Chemical Engineering, 25, 6, 1444, 2008.

[142] Y. N. Xue, Z. Z. Huang, J. T. Zhang, M. Liu, M. Zhang, S. W. Huang, R. X. Zhuo, Polymer, 50:15, 3706, 2009.

[143] G. H. Li, P. P. Yang, Z. S. Gao, Y. Q. Zhu, Colloid Polymer Science, 290, 1825, 2012.

[144] L. Luo, A. Eisenberg, Langmuir, 17, 6804, 2001.

[145] L. Luo, A. Eisenberg, Journal of American Chemistry Society, 123, 1012, 2002.

[146] J. M. Weissman, H. B. Sunkara, A. S. Tse, S. A. Asher, Science, 274, 959, 1996.

[147] S. A. Rice, Chemical Physics Letters, 479, 1, 2009.

[148] J. Hostomskp, Z. Halasz, I. Liszi, J. Npvlt, Powder Technology, 49, 45, 1986.

[149] B. W. Longbottom, B. Somuncuog˘lu, J. J. Punter, S. Longbottom, S. A. F. Bon, Soft Matter, 13, 4285, 2017.

[150] A. R. Denton, Q. Tang, The Journal of Chemical Physics, 145, 164901, 2016.

[151] D. P. Rozairo, A. B. Croll, Langmuir, 31, 1308, 2015.